



City Research Online

City St George's, University of London

Citation: Ferreira, F. P. V., Tsavdaridis, K. D., Martins, C. & De Nardin, S. (2021). Ultimate strength prediction of steel–concrete composite cellular beams with PCHCS. *Engineering Structures*, 236, 112082. doi: 10.1016/j.engstruct.2021.112082

This is the accepted version of the paper.

This version of the publication may differ from the final published version. To cite this item please consult the publisher's version.

Permanent repository link: <https://openaccess.city.ac.uk/id/eprint/27684/>

Link to published version: <https://doi.org/10.1016/j.engstruct.2021.112082>

Copyright and Reuse: Copyright and Moral Rights remain with the author(s) and/or copyright holders. Copies of full items can be used for personal research or study, educational, or not-for-profit purposes without prior permission or charge, unless otherwise indicated, provided that the authors, title and full bibliographic details are credited, a hyperlink and/or URL is given for the original metadata page and the content is not changed in any way. For full details of reuse please refer to [City Research Online policy](#).

Ultimate strength prediction of steel-concrete composite cellular beams with PCHCS

Felipe Piana Vendramell Ferreira^{*a}, Konstantinos Daniel Tsavdaridis^b, Carlos Humberto Martins^c, Silvana De Nardin^a

^aDepartment of Civil Engineering, Federal University of São Carlos, Rod. Washington Luiz, km 235, São Carlos, São Paulo, Brazil.

^bSchool of Civil Engineering, Faculty of Engineering and Physical Sciences, University of Leeds, Woodhouse Lane, LS2 9JT Leeds, UK.

^cDepartment of Civil Engineering, State University of Maringá, Av. Colombo n° 5790, Maringá, Paraná, Brazil.

*Corresponding author

E-mail address: fpiana@live.com (F. P. V. Ferreira), K.Tsavdaridis@leeds.ac.uk (K. D. Tsavdaridis), chmartins@uem.br (C. H. Martins), snardin@ufscar.br (S. De Nardin)

Abstract

This paper aims to predict the ultimate behavior of steel-concrete composite cellular beams with precast hollow core slabs. A finite element model is developed by geometrical non-linear analysis. A parametric study is carried out, considering symmetric and asymmetric sections with precast hollow core slabs. The key parameters such as the web-post width and the opening diameter are varied, as well as the presence of the concrete topping. A total of 120 analyses were performed. The results are compared with composite slab models. For symmetrical sections, considering the hollow core slabs, although some observations occurred with the formation of the plastic mechanism, the predominant failure mode was the web post buckling. For asymmetric sections, the predominant failure mode was the combination of the plastic mechanism with the web post buckling, which were accompanied by the shear connector rupture. In both cases, considering symmetrical and asymmetrical sections, excessive cracking was observed in the upper part of the hollow core slab. In cases where the end post was greater than the web post, there was damage at the upper region of the hollow core slab/concrete topping, close to the support. The numerical models of composite cellular beams with hollow core slabs, when compared with the models of composite cellular beams with composite slabs, showed greater efficiency in structural behavior. The differences observed between the shear strengths of the analyzed models, considering hollow core slab and composite slab, hollow core slab with concrete topping and composite slab, and hollow core slab with concrete topping and hollow core slab were 33kN, 121kN and 92kN, respectively, considering symmetric sections. For the asymmetric sections, such differences were 81kN, 103kN and 76kN, considering hollow core slab and composite slab, hollow core slab with concrete topping and composite slab, and hollow core slab with concrete topping and hollow core slab, respectively. These results imply that the strength of the composite cellular beams was not limited only by the strength of the steel cellular beam, but also, of the slab, due to the resistance to shear stress.

Keywords: Cellular beams; Precast hollow core slabs; Concrete topping; Geometrical nonlinear analyses.

33 NOTATION

34 The following symbols are used in this paper:

HCU	Hollow core unit	M_i	moment at i opening
PCHCS	Precast hollow core slab	M_{vh}	moment generated by horizontal shear force
PCHCSCT	Precast hollow core slab with concrete topping	$M_{W,e}$	elastic bending moment of web post
b	the width of the concrete slab	$M_{W,Rk}$	flexural strength of Ward's model;
b_f	the width of the flange	t_f	the thickness of the flange
b_w	the width of the web post	t_w	the thickness of the web
b_{we}	the width of the end post	V	the global shear force
C_i	the axial force in concrete of a composite section	V_h	the horizontal shear force
C_1	the dimensionless constant in Eq. (26)	y_o	the distance from the geometric center of the tee to bottom edge
C_2	the dimensionless constant in Eq. (27)	$y_{o,inf}$	the distance from the geometric center of the bottom tee to bottom edge
C_3	the dimensionless constant in Eq. (28)	β_c	the dimensionless constant in Eqs. (3-4)
D_o	the opening diameter	ε	strain
d	the depth of parent section;	ε_c	the compressive strain
d_{eff}	the effective depth of composite cellular beam	ε_t	the tensile strain
d_g	the depth of cellular beam	$\bar{\lambda}$	reduced slenderness factor
f_c	the compressive cylinder strength of concrete	λ_w	web slenderness ratio
$f_{c,PCHCS}$	the compressive cylinder strength of precast hollow core slab	μ	the viscosity parameter that represents the relaxation time
f_s	the yield strength of transversal reinforcement	ζ	the eccentricity (defines the rate at which the function approaches the asymptote, the default value is 0.1)
f_t	the concrete tension resistance	σ	stress
f_u	the ultimate strength of cellular beam	σ_{b0}	the initial equibiaxial compressive yield stress
f_y	the yield strength of cellular beam	σ_{c0}	the initial uniaxial compressive yield stress
K_c	the ratio of the second stress invariant on the tensile meridian to that on the compressive meridian, $0.5 \leq K_c \leq 1.0$	φ	the diameter of transversal reinforcement
L_b	the unrestrained length of composite cellular beam	χ	reduction factor
L_p	the distance between support and load	Ψ	dilation angle
l_{eff}	effective length of web-post		
p	the length between the opening diameter centers		

35

36

37

38

1. INTRODUCTION

Steel-concrete composite beams associated with the cast in-situ concrete slabs, i.e. solid or composite slabs, possess some disadvantages such as the high operational cost of welding the shear connectors and the curing time of wet concrete in cold climates. To reduce such limitations, the use of precast concrete hollow core slabs (PCHCS) can be an alternative [1]. These elements are produced in specific environments with monitoring and strict technological control. The use of PCHCS offers advantages such as the possibility of overcoming large spans, speed, and reduced construction costs [2–4]. One of the common uses of PCHCS is in flooring systems. Generally, a concrete topping is made to provide resistance to actions and a smooth and uniform finish [5,6].

With the development of automated cutting and welding from the 1990s, cellular beams started to be manufactured at low costs, thus expanding the product in the civil construction market. Cellular steel beams are produced by means of two thermal cut lines, in the shape of semi-circles, along the entire longitudinal web length. Subsequently to the thermal cutting step, the parts are separated and then welding (Fig. 1). These beams are ideal for structures with open space requirements such as parking garages, industries and warehouses, factories, office buildings, schools and hospitals. In addition, cellular beams are a good solution to overcome large spans and reduce the structure's own weight.

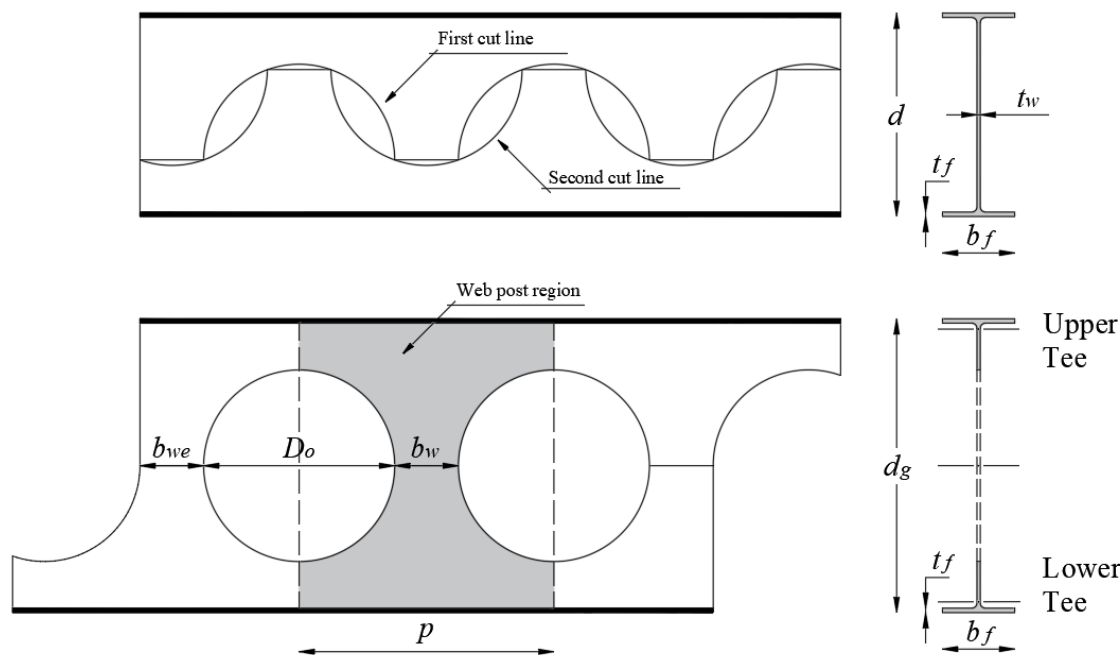
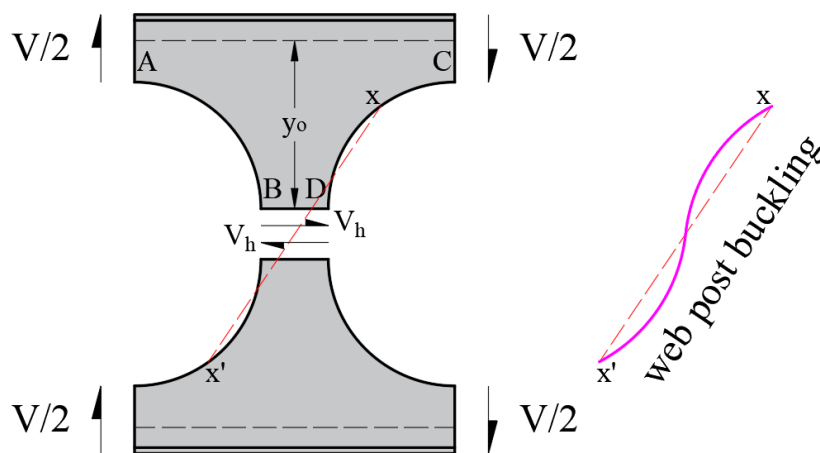


Fig. 1: Cellular beams manufacturing process [7]

Regarding their structural behavior, the strength of the composite cellular beams is associated with the failure mechanisms of the slab, i.e. cracking or crushing, combined with those of the cellular beams, such as the web post buckling (WPB) and the Vierendeel mechanism (VM). The WPB phenomenon becomes critical when the web post width is reduced [8–11]. As shown in Fig. 2 [12], a horizontal shear force (V_h) acts along the welded joints, where y_0 is the distance from the geometric center of the tee section to the weld, and V is the global shear force. In the exemplified case, the AB edge is requested by tensile stresses, while the CD edge is requested by compressive stresses. As a result, the flexural behavior will arise in web post. This phenomenon is

60 characterized by a double curvature (in the shape of "S"). On the other hand, the VM is dependent on the presence of high magnitude
 61 shear force, and it is a phenomenon characterized by the distortion and formation of plastic hinges in regions close to the opening
 62 [13,14]. Physically, VM occurs when the ends of the tees reach the yield strength due to the combination of normal and tangential
 63 stresses. The main parameters that affect this structural behavior are the web thickness, the effective opening diameter and the
 64 number of shear connectors allocated above the opening (composite action) [12,15–19].



65
66 **Fig. 2: Web post buckling (WPB), adapted from [12]**

67 From the design point of view, desirable characteristics of the steel-concrete composite beams are still unquestionable. It
 68 is a structural system with widespread use worldwide and with very consolidated calculation procedures. Thus, if steel-concrete
 69 composite beams, PCHCS and steel profiles are structural elements with very interesting aspects for use in multi-storey buildings,
 70 the cellular section combination working together with the PCHCS is interesting and promising. However, it is not an association
 71 that has been investigated by the scientific community, and although the SCI-P355 [19] and Steel Design Guide 31[20]
 72 recommendations are directed at the behavior of composite beams with web openings, such recommendations are limited in the use
 73 of composite slabs [21]. The present study aims to predict the ultimate behavior of steel-concrete composite cellular beams with
 74 precast hollow core slabs. Three types of slabs are studied; PCHCS (LP15) with and without concrete topping, and a composite slab
 75 with the Holorib 51/150 steel sheets geometry. Due to limitations of the steel sheets, 150mm spacing between connectors is
 76 considered. A finite element model is developed by geometrical nonlinear analyses. The numerical model is calibrated, considering
 77 tests. A parametric study is carried out. The steel-concrete composite beams are simply supported, with a span of 6m. Symmetric
 78 (IPE 400) and asymmetric (IPE 400/HEB 340) sections are considered. For each section, the influence of the slab type is studied,
 79 and the key parameters such as the web-post width and the opening diameter are varied. The results are discussed, according to the
 80 parameters presented.

81 2. BACKGROUND

82 In this section, research studies are presented considering steel-concrete composite beams with PCHCS and composite
 83 cellular beams. In late 90's, Lam [22] studied the steel-concrete composite beams with PCHCS, considering pushout tests, as well
 84 as the flexural behavior. Subsequently, several studies were published. [3,23–26]. In Lam et al. [24] results of flexural tests were

85 presented. The ductile behavior was observed, which can be controlled by the appropriate use of transverse reinforcement and in
86 situ concrete strength. Lam et al. [25] complemented the previous study, using the finite element method to develop a parametric
87 analyses. In this study, it was reported that increasing the transverse reinforcement rate, significantly increases the flexural strength,
88 but reduces the ductility leading to the fragile rupture of the concrete slab; the higher the slab depth, the greater the resistant moment,
89 although the slab may fail due to excessive cracking. In 2003, Steel Construction Institute published SCI-P287 [27], which is a
90 manual containing design criteria for composite beams with PCHCS. Subsequently, the SCI-P401 [28] was published, which is an
91 update of the previous document. In this publication, recommendations are presented, considering the minimum dimensions,
92 arrangement of headed stud connectors, transverse reinforcement rate, ultimate, and service limit states in the construction phase
93 for the cases of full and partial interaction. Such publication is based on EC4 [29]. Batista and Landesmann [30] tested composite
94 beams with PCHCS and concrete topping. The tests showed similar collapse modes, with the development of cracks initiated on the
95 underside of the HCU and in the central region between the load application points. According to the authors, these cracks
96 propagated along the width of the PCHCS, extending from the side face of the slab to the region of connection with the steel profile,
97 a factor that reduced the stiffness of the composite beam. In Ferreira et al. [31] a parametric study of composite beams with PCHCS
98 and concrete topping was presented. In this study, as observed in [5,6], the concrete topping increased the initial stiffness of the
99 composite beams, as well as its ultimate strength.

100 On the other hand, considering composite cellular beams, the studies dated back to the early 2000s. In the literature there
101 are studies considering composite beams with only a rectangular web opening with solid [32–39] or composite slabs [13,37–48],
102 and composite plug systems with perforated beams [52–56]. In the latter case, one of the benefits is that WPB and VM cannot be
103 achieved as the thin-walled perforated section with large closely spaced web opening is partially encased by concrete (one opening
104 every other metal deck rib) which also acts as a shear connector with the concrete passing through. The present study focuses on
105 cellular beams, which are those with periodical circular web openings, according to the manufacturing process shown in **Fig. 1**. In
106 this scenario, several studies have investigated the behavior of composite cellular beams with asymmetric section [7,57–60].
107 Sheehan et al. [60] described that the asymmetric composite beams has been widely used in construction. The main advantage of
108 using these elements is that the lower tee is formed by a more rigid section than the upper tee, to increase the resistance to bending
109 and shearing. In Müller et al. [58] tests of two models were presented: composite symmetric and asymmetric cellular beams. Both
110 specimens were designed in such a way that at one end it was possible to investigate the composite action, and at the other end, only
111 the cellular section. The ultimate behavior of the tests was similar. According to the authors, the VM was observed for low loading
112 values at the end corresponding to the composite action. Oppositely, at the end where there was only the cellular steel profile, the
113 ultimate strength was reached by WPB. To explore a larger number of observations, the authors performed a parametric study to
114 investigate the influence of the resistance of steel and concrete materials on the strength of the physical models. According to the
115 authors, the resistance of the cellular profile is preponderant in the ultimate strength of composite cellular beams, since the it was
116 reached by the WPB. Also, Nadjai et al. [59,61] examined composite symmetric and asymmetric cellular beams. Both models had

the ultimate strength governed by WPB. Sheehan et al. [60] tested long spanning asymmetric composite cellular beams. The interaction degree considered was lower than that recommended in EC4 [29]. The composite asymmetric cellular beams were subjected to uniformly distributed loads and concentrated loads, which were applied to 5/16 and 7/16 of the span length. The slip in the steel-concrete interface, the vertical displacements, the stress distribution, and the effect of the unscored construction were evaluated in the study. The authors observed that the composite cellular beams submitted to uniformly distributed loading resisted 3.4 times the estimated design load, despite the interaction degree considerably less than the minimum required by EC4 [29]. The composite cellular beam that was subjected to concentrated load had its strength 45% greater than that resisted by the cellular profile. This suggests the need for modifications in the prediction of resistance to the VM. In Ferreira et al. [7] the resistance of steel-concrete composite cellular beams was investigated by geometric nonlinear analyses. The key parameters such as the opening diameter and the web post width were varied. The authors concluded that the end post and the concrete slab contributed significantly to the shear strength of composite cellular beams. Thus, it is possible to state that, to date, there are no studies of composite cellular beams with PCHCS.

3. FINITE ELEMENT MODEL: VALIDATION STUDY

For the validation study, seven steel-concrete composite beams are modeled, considering symmetry (Fig. 3). Geometrical nonlinear analyses are processed using the ABAQUS® [62] software. The analyses are divided into two groups:

- Steel-concrete composite beams with hollow core slabs are processed in one step, considering the *Static Riks* analysis [31]. In this analysis, initial geometric imperfections are not considered, since the ultimate behavior of these structures is governed only by plastification of the steel profile, or crushing and cracking of the concrete slab. At the beginning of the analysis, it is necessary to implement the initial arc length, which refers to an initial percentage of the external load. Thus, in the next increments, the software, automatically during the analysis, adjusts the load increments so that the problem converges [62]. This type of analysis was also used in [22,31,63,64].
- Steel-concrete composite cellular beams are processed in two steps: *Buckle* and *Static Riks* analyses [7,65–68]. *Buckle* analysis is used to estimate critical buckling loads in structures by obtaining eigenvalues and their eigenvectors. It is important to note that in this type of analysis, no imperfections, physical and geometric, are considered in the structure. In the second step, the *Static Riks* analysis is performed considering non-linear geometrical and material analysis. In the case of cellular beams, the initial geometric imperfection is imposed. The implementation of geometric imperfection is performed using the command *INITIAL CONDITIONS. It is important to note that residual stresses were not considered. This is due to the fact that these stresses do not influence the composite beams subjected to positive bending moment. Otherwise, when the composite beams are subjected to a negative bending moment, residual stresses are harmful, and the structure can reach the ultimate behavior by distortional buckling [69,70]. As described in [8], in cellular beams the initial imperfections are inevitable due to the manufacturing process, and therefore, it is a difficult task to be determined. In this way, the initial geometric imperfection factor was applied by a scale factor equal to $d_g/1000$, according to sensitivity analyses performed by Ferreira et al. [7].

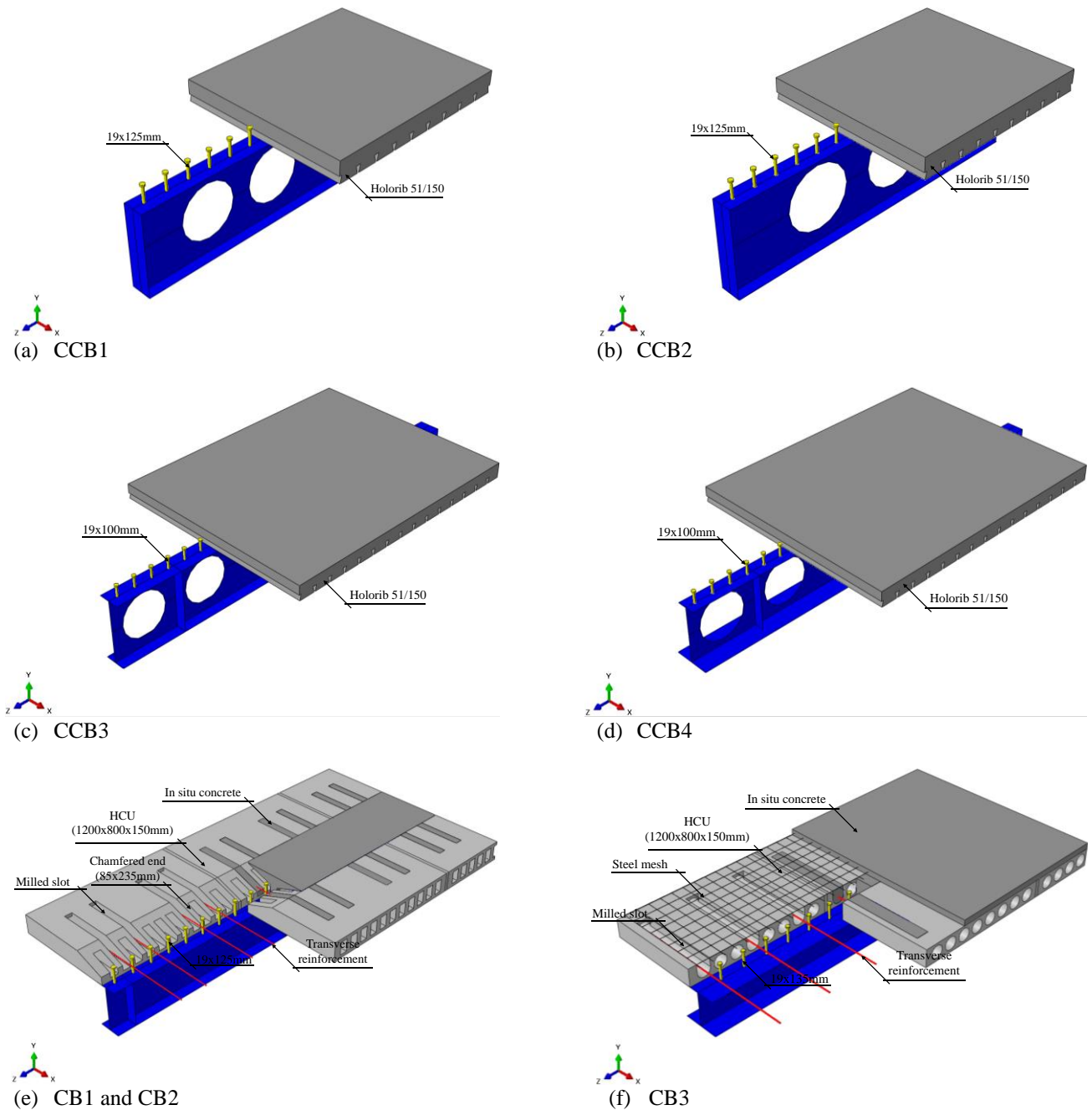


Fig. 3: Steel-concrete composite beams for the validation study, considering symmetry

3.1. TESTS

With regard to composite cellular beams, the tests results of models 1A (CCB1), 1B (CCB2), RWTH-1A (CCB3) and RWTH-1A (CCB4) were considered for the validation study [57–59,61]. It is worth mentioning that, although the steel sheets were not modeled, the Holorib HR 51/150 geometry was used to represent the concrete slab ribs. The headed stud connectors dimensions are 19x120mm (CCB1 and CCB2) and 19x100mm (CCB3 and CCB4), spaced at 150mm. For the composite beams with PCHCS, the numerical model validation was based on tests results of Lam [22], and Batista Landesmann [30]. In the models CB1 and CB2 [22], the HCU dimension were 1200x800x150mm, with a chamfer. The 19x125mm headed stud connectors were spaced in 150mm. On the other hand, in the CB3 model [30], the HCU dimension were 1200x800x150mm with a 50mm thick concrete topping,

158 reinforced with Q138 steel mesh (4.2x100x100). The 19x135mm shear connectors were spaced in 200mm. In **Table 1**, the details
159 of the models are presented.

160 **Table 1: Models (in mm, MPa and GPa)**

Model	Ref	d or d_s	D_o	p	Upper tee					Lower tee					E	Slab		Reinforcement		b	L_b	L_p
					b_f	t_f	t_w	f_y (flange/web)	f_u (flange/web)	b_f	t_f	t_w	f_y (flange/web)	f_u (flange/web)		f_c	$f_{c,PCHCS}$	φ	f_s			
CCB1	[59]	575	375	500	141.8	8.6	6.4	312	438.5	141.8	8.6	6.4	312	438.5	200	28.6	-	-	-	1200	4500	1750
CCB2	[59]	630	450	630	141.8	8.6	6.4	312	438.5	152.4	10.9	7.6	312	438.5	200	28.6	-	-	-	1200	4500	2250
CCB3	[58]	555	380	570	180	13.5	8.6	451/489	541/587	180	13.5	8.6	451/489	541/587	195	33.6	-	-	-	1800	6840*	1140/2850
CCB4	[58]	485	380	570	150	10.7	7.1	407/467	524/588	300	21.5	12	453/488	519/582	195	24.0	-	-	-	1800	6840*	1140/2850
CB1	[64]	355	-	-	171.5	11.5	7.4	310/355	$1.3f_y$	171.5	11.5	7.4	310/355	$1.3f_y$	205	25.6	40	16	585	1665	5700	1500
CB2	[64]	355	-	-	171.5	11.5	7.4	310/355	$1.3f_y$	171.5	11.5	7.4	310/355	$1.3f_y$	205	20.8	40	8	473	1665	5700	1500
CB3	[30]	299	-	-	306	11	11	345	450	306	11	11	345	450	200	30.0	45	12.5	500	1756	5830	1915

161 *Slab cut back by 285 mm at end of cellular beam

3.2. MATERIALS MODELS

In this section, the materials constitutive models used in numerical modeling are presented.

3.2.1 Concrete

The Concrete Damage Plasticity (CDP) [71–73] is adopted. The model takes into account hypotheses based on the theory of plasticity [74], and the stress-strain relationship is governed by a damaged elastic variable. The damage variables can take values from 0 (undamaged material) to 1 (total loss of strength). The **Eq. (1)** and **Eq. (2)** represents the damage variable, considering the concrete in compression and tension, respectively.

$$d_c = 1 - (\sigma / f_c) \quad (1)$$

$$d_t = 1 - (\sigma / f_t) \quad (2)$$

The CDP makes use of the resistance function of Lubliner et al. [72], with the modifications proposed by Lee and Fenves [73] to explain the different evolution of resistance under tension and compression. This function defines the direction of the deformations, when the material reaches the state of plastic behavior. The input parameters to characterize the plasticity are: dilation angle (ψ), eccentricity (ξ), the ratio of initial equibiaxial compressive yield stress to initial uniaxial compressive yield stress (σ_{b0}/σ_{c0}), the ratio of the second stress invariant on the tensile meridian to that on the compressive meridian (K_c), and the viscosity parameter that represents the relaxation (μ). **Table 2** presents the input parameters for defining the plastic behavior.

Table 2: CDP input parameters

Parameter	Value
Ψ (°)	40
ξ	0.1 (default)
σ_{b0}/σ_{c0}	1.16 (default)
K_c	2/3 (default)
μ (s ⁻¹)	0.001

The Carreira and Chu [75,76] models were adopted to represent the behavior of concrete in compression and tension, according to **Eqs. (3-5)**.

$$\frac{\sigma}{f_c} = \frac{\beta_c (\varepsilon / \varepsilon_c)}{\beta_c - 1 + (\varepsilon / \varepsilon_c)^{\beta_c}} \quad (3)$$

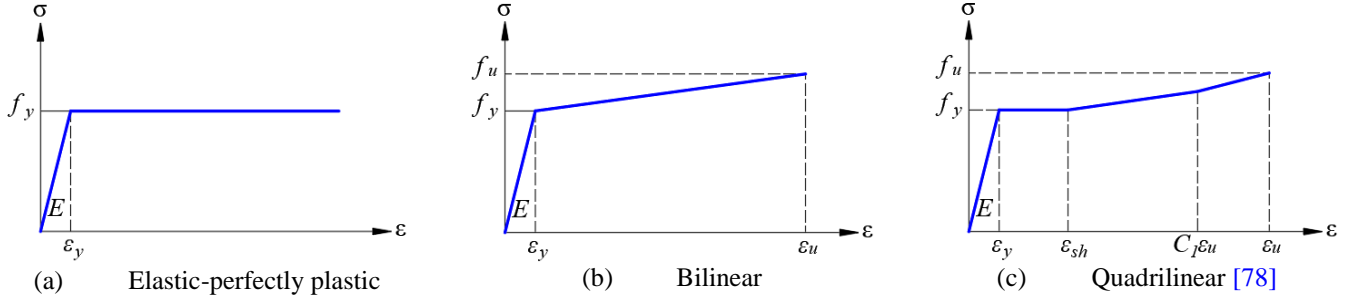
$$\frac{\sigma}{f_t} = \frac{\beta_c (\varepsilon / \varepsilon_t)}{\beta_c - 1 + (\varepsilon / \varepsilon_t)^{\beta_c}} \quad (4)$$

$$\beta_c = \left(\frac{f_c}{32.4} \right)^3 + 1.55 \text{ (MPa)} \quad (5)$$

3.2.2 Steel

For the transverse reinforcement and steel mesh, the elastic-perfectly plastic model was adopted (**Fig. 4a**). Regarding the headed stud connectors, the bilinear model was used [77] (**Fig. 4b**), i.e., the yield stress and the ultimate stress were 460 MPa and 559 MPa, respectively. The elongation at rupture was 18.8%. For the structural steel profiles, the quadrilinear model of Yun and

182 Gardner was used [78] (Fig. 4c). According to the authors, the quadrilinear diagrams are more accurate and they are in accordance
 183 with the experimental stress-strain curves across the tensile stress range. The model parameters are calculated, according to the
 184 Eqs. (4-8). The implementation of the stress-strain relationship must be done with the real values, according to the Eqs. (6-12).
 185
 186



187

Fig. 4: Stress-strain relationship for steel

$$f(\varepsilon) = \begin{cases} E\varepsilon, \varepsilon \leq \varepsilon_y \\ f_y, \varepsilon_y < \varepsilon \leq \varepsilon_{sh} \\ f_y + E_{sh}(\varepsilon - \varepsilon_{sh}), \varepsilon_{sh} < \varepsilon \leq C_1\varepsilon_u \\ f_{C_1\varepsilon_u} + \left(\frac{f_u + f_{C_1\varepsilon_u}}{\varepsilon_u - C_1\varepsilon_u} \right), C_1\varepsilon_u < \varepsilon \leq \varepsilon_u \end{cases} \quad (6)$$

$$\varepsilon_u = 0.6 \left(1 - \frac{f_y}{f_u} \right), \varepsilon_u \geq 0.06 \quad (7)$$

$$\varepsilon_{sh} = 0.1 \frac{f_y}{f_u} - 0.055, 0.015 < \varepsilon_{sh} \leq 0.03 \quad (8)$$

$$C_1 = \frac{\varepsilon_{sh} + 0.25(\varepsilon_u - \varepsilon_{sh})}{\varepsilon_u} \quad (9)$$

$$E_{sh} = \frac{f_u - f_y}{0.4(\varepsilon_u - \varepsilon_{sh})} \quad (10)$$

$$\sigma^{true} = \sigma^{nom} (1 + \varepsilon^{nom}) \quad (11)$$

$$\varepsilon^{true} = \ln(1 + \varepsilon^{nom}) \quad (12)$$

188 3.3. INTERACTION

189 Three types of interaction were considered [62]:

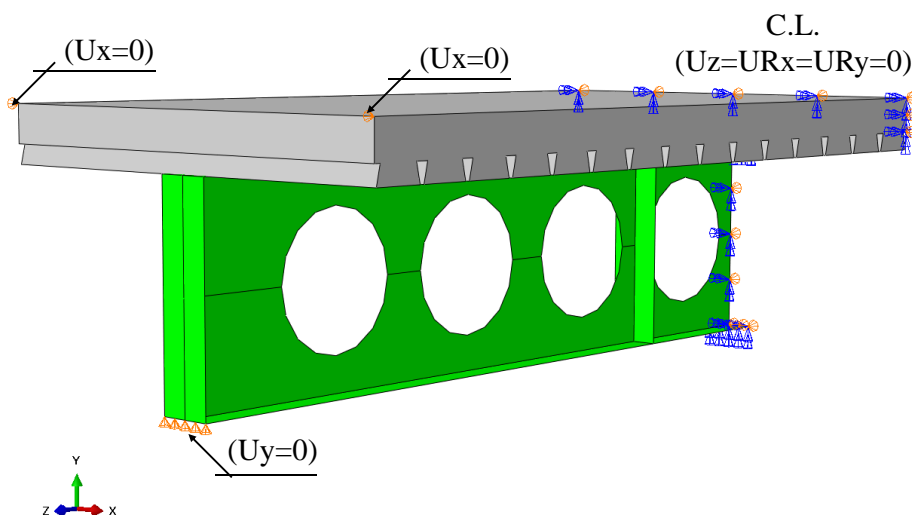
- 190 i. *Tie constraint (surface-to-surface)*: this modeling technique allows to simulate the perfect bond between the contact surfaces.
 191 In this case, each node on the slave surface will have the same values for its degrees of freedom as the point on the master
 192 surface;
- 193 ii. *Embedded*: this type of interaction is used to specify that an element is embedded in another element;

194 iii. *Normal/tangential behavior (surface-to-surface)*: allows displacement in the normal and tangential direction to the contact
 195 surface plane.

196 The tie constraint was applied to the surface between on the bottom surfaces of the shear connectors and the upper flange,
 197 and between the precast and in-situ infill concrete [31]. The contact between the concrete and the transverse reinforcement, as well
 198 as the concrete and steel mesh, were made through the embedded region. The shear connectors were represented in the modeling
 199 and allocated in the concrete volume of the slab. In this methodology, the same volume of the shear connector is cut from the slab
 200 [79,80]. The purpose of this volume removal is such that the interaction between the contact surfaces of the slab and the shear
 201 connector occurs. The tangential behavior is based on the Coulomb friction model. According to the literature, the coefficient of
 202 friction between the steel and concrete surfaces varies between 0.2 to 0.83 [63,81–83]. Guezouli and Lachal [82] performed
 203 sensitivity analyses, via finite element method to investigate the mechanical behavior at the steel-concrete interface, considering
 204 pushout tests. In this study, the friction coefficients were varied by 0.1, 0.2, 0.3, 0.4 and 0.5, both for the interface between the
 205 connectors and the concrete slab, and for the interface between the concrete slab and the steel profile. The results were compared
 206 with tests. The authors recommended the use of the values of the friction coefficients equal to 0.2 and 0.3 for the interfaces between
 207 the connector-slab and slab-profile, respectively. Therefore, for the validation of the numerical model of the present work, the
 208 recommendation of Guezouli and Lachal [82], that is, for CCB1, CCB2, CCB3, CCB4, CB1, CB2 and CB3 models, the friction
 209 coefficients were assumed equal to 0.2 and 0.3, for headed stud and slab interface, and slab and steel profile interface, respectively.

211 3.4. BOUNDARY CONDITIONS

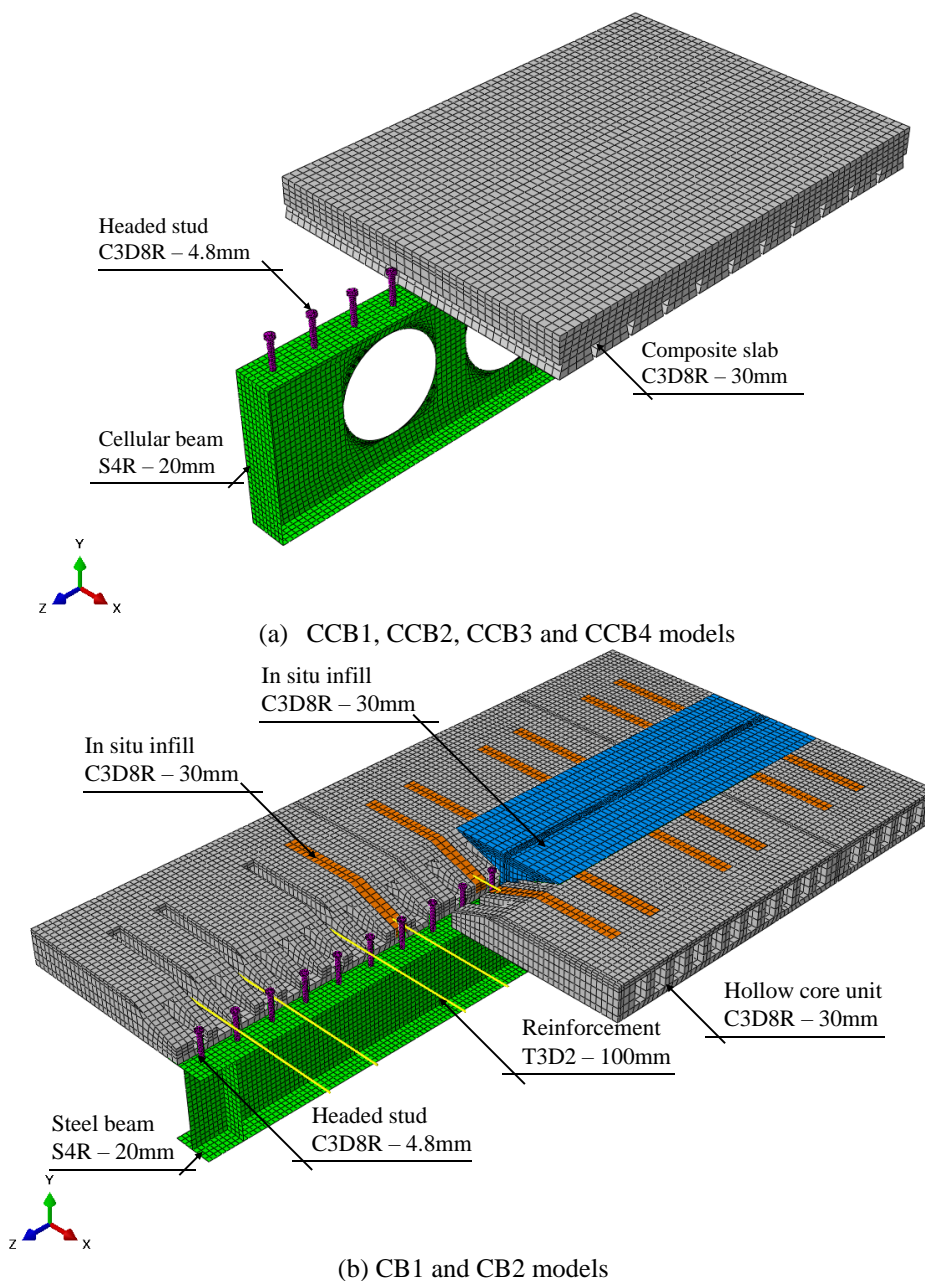
212 The boundary conditions were applied considering the symmetry at the longitudinal axis [7,31]. Vertical displacement
 213 ($U_y=0$) in the support, and lateral displacement ($U_x=0$) at the ends of the slab were restrained. Longitudinal symmetry was applied
 214 at mid-span by restrictions to longitudinal displacement, rotation around the x and y axis ($U_z=U_{R_x}=U_{R_y}=0$). **Fig. 5** shows the
 215 boundary conditions that was applied in all models.

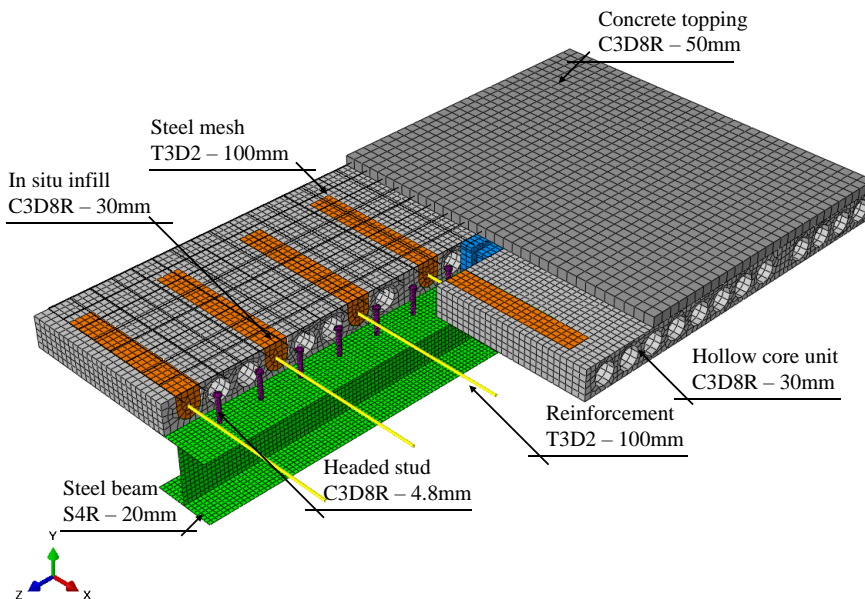


216
217 **Fig. 5: Boundary conditions**

3.5. DISCRETIZATION

Fig. 6 illustrates the discretization of the models. The dimension of the elements was taken according to previous studies [63,81,84] respecting the master and slave surfaces. The assignment of master and slave roles can have a significant effect on performance with surface-to-surface contact if the two surfaces have dissimilar mesh refinement; the solution can become quite expensive if the slave surface is much coarser than the master surface [62]. The steel profiles were discretized with shell-type finite elements. The S4R element is a quadrilateral element with four nodes and reduced integration. The headed stud connectors, the concrete slab, as well as the in-situ elements, were discretized by the solid element C3D8R, which has eight nodes, reduced integration, supports plastic analysis with large deformations, and allows the visualization of the crack in the CDP model. Both elements have six degrees of freedom per node - three rotations and three translations. The transverse reinforcement and the steel mesh were discretized by T3D2 truss elements, with two nodes and linear displacement.



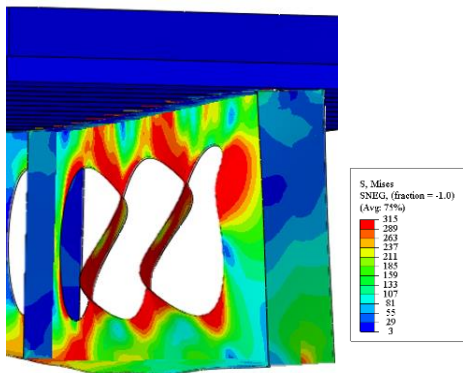


(c) CB3 model

Fig. 6: Discretization

3.6. VALIDATION RESULTS

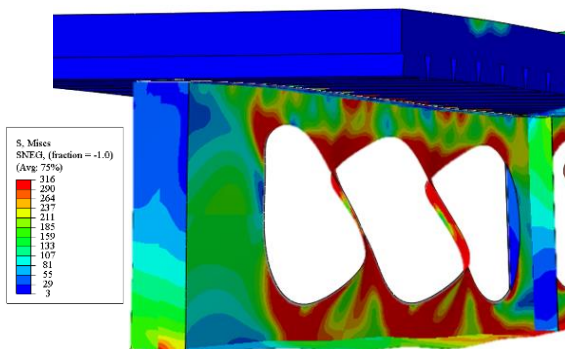
In this section, the results of the numerical validation with the tests are discussed. Considering the models CCB1 and CCB2, both had the ultimate behavior defined by WPB, as shown in Nadjai [59] and Nadjai et al. [61]. Fig. 7a-d shows the comparison of the deformation of the numerical models with the tests. Fig. 9a-b shows the results of load per displacement, of models CCB1 and CCB2, respectively. Considering the CCB3 and CCB4 models, the failure modes were similar to that described by Hechler et al. [57] and Müller et al. [58]. According to the authors, the yield strength reached for low levels of loading in the openings, and the ultimate behavior was governed by WPB. Fig. 7e shows the deformation of CCB3 and CCB4 models. The ultimate behavior of models CB1, CB2 and CB3 are also shown. The failure modes of the CB1 and CB2 models were similar (Fig. 8a). As described by Lam [22], in the CB1 and CB2 models it was possible to observe the plastification of the lower flange and the excess of cracking in the lower part of the hollow core slab. The CB3 model (Fig. 8b), on the other hand, showed excessive cracking, mainly at the load application point, at the bottom of the hollow core slab. Such cracks extended to the sides of the slab, as described by Batista and Landesmann [30]. Fig. 5 illustrates the response of the numerical models developed in comparison to the tests. Table 3 shows the results. For models CCB1, CCB2, CCB3 and CCB4, the post buckling analysis ended when the structures reached WPB. For the CB1, CB2 and CB3 models, there was iterative solution technique failure as a convergence problem. In this case, the CB1, CB2 and CB3 models, this behavior reached with excessive cracking (material failure).



(a) WPB for CCB1 model



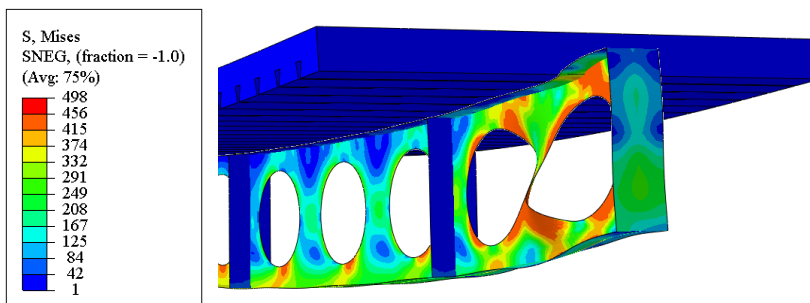
(b) Test CCB1 [59]



(c) WPB for CCB2 model



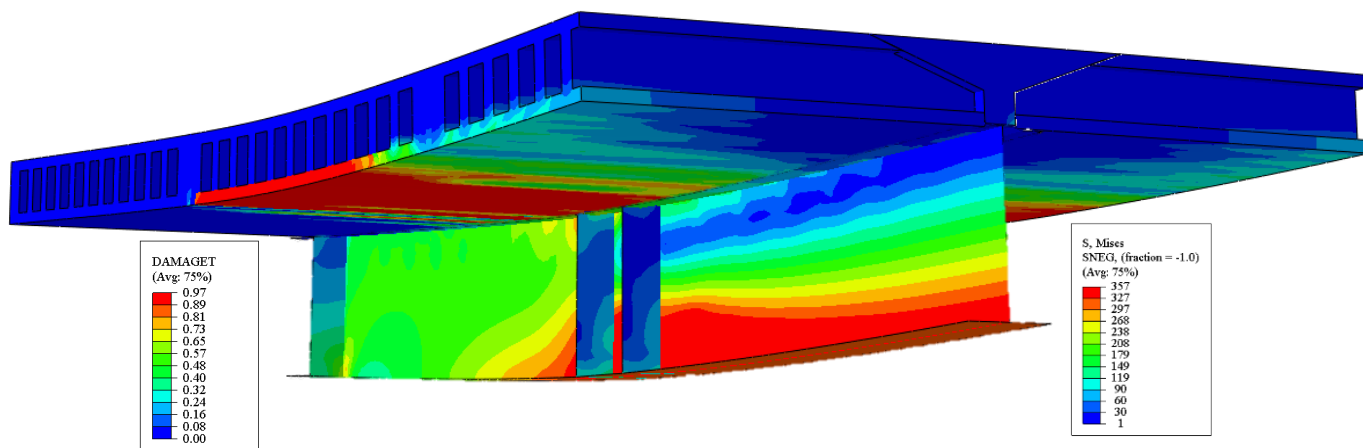
(d) Test CCB2 [59]



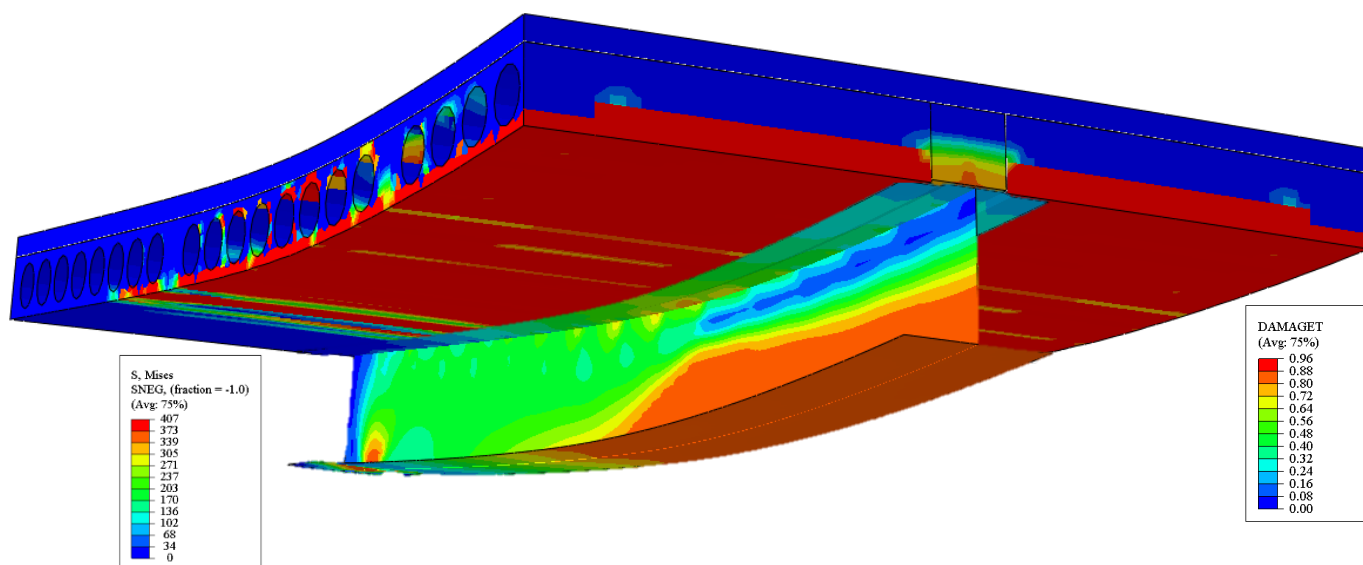
(e) WPB for CCB3 and CCB4 models

Fig. 7: Ultimate behavior of CCB1, CCB2, CCB3 and CCB4 models

248
249
250
251
252
253
254
255
256
257
258



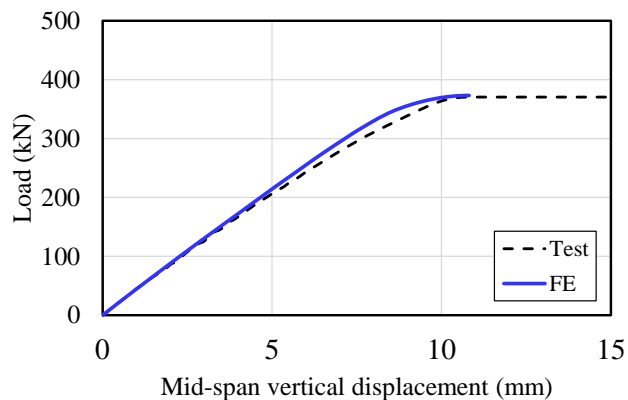
(a) CB1 and CB2 models



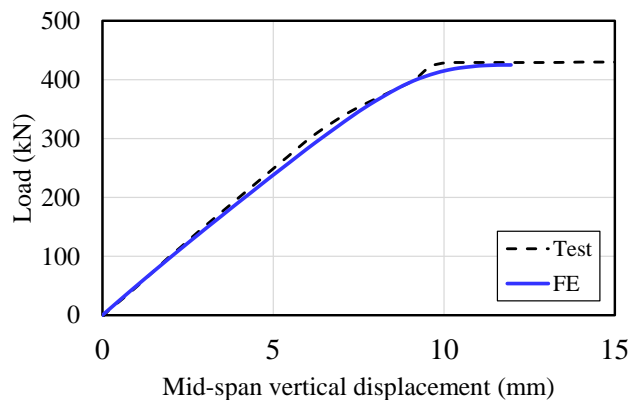
(b) CB3 model

Fig. 8: Ultimate behavior of CB1, CB2 and CB3 models

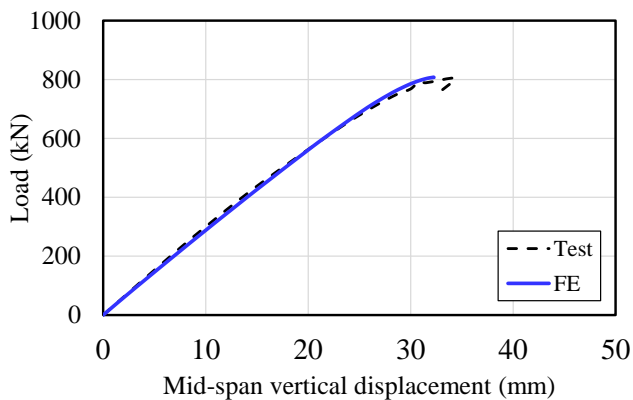
259
260
261
262
263
264
265
266
267
268
269
270



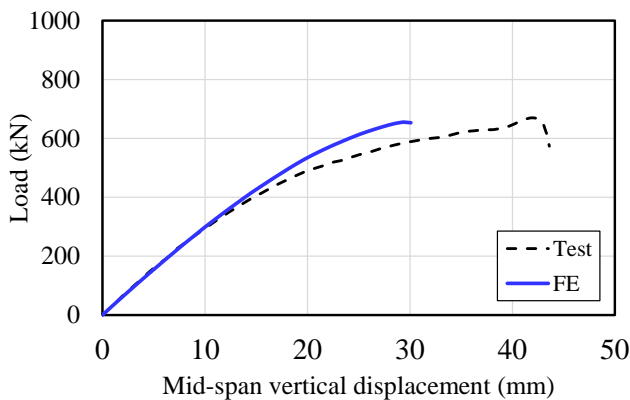
(a) CCB1



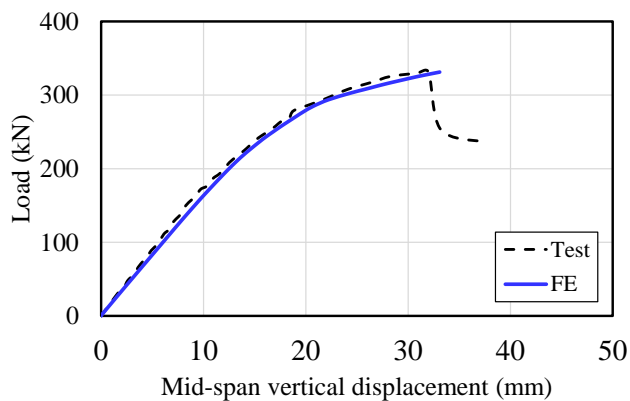
(b) CCB2



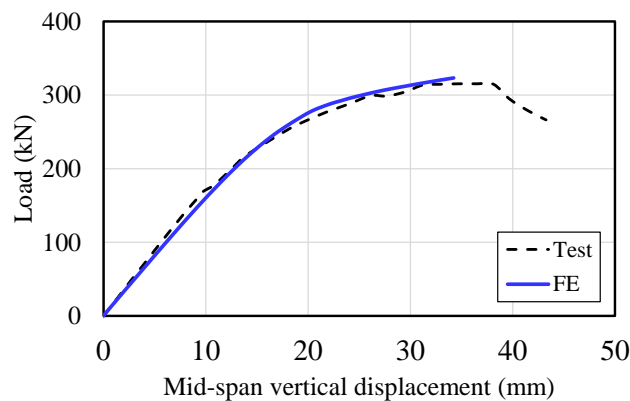
(c) CCB3



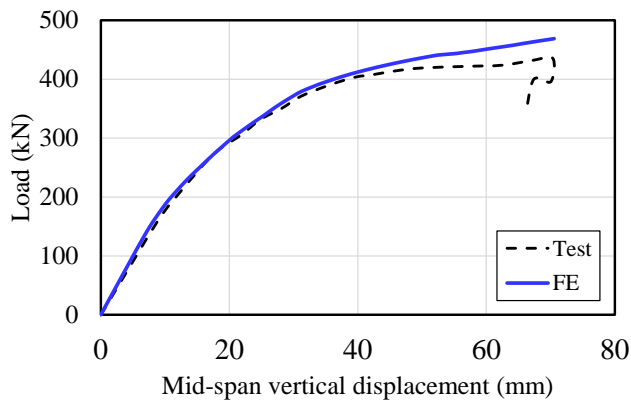
(d) CCB4



(e) CB1



(f) CB2



(g) CB3

Fig. 9: Validation results

271

272

273

Table 3: Summary of results

Model	P_{Test} (kN)	P_{FE} (kN)	P_{FE}/P_{Test}
CCB1	370	373	1.01
CCB2	430	425	0.99
CCB3	806	808	1.00
CCB4	658	655	1.00
CB1	331	331	1.00
CB2	316	323	1.02
CB3	442	469	1.06
Average			1.01
S.D			2.17%
COV			0.05%

4. FINITE ELEMENT MODEL: PARAMETRIC STUDY

In view of the results obtained, it is possible to state that the numerical model is calibrated. Thus, as the composite cellular beams with PCHCS are similar structures to the models used in the validation study, it is possible to develop a numerical model to predict the ultimate behavior of these composite beams (**Fig. 10**).

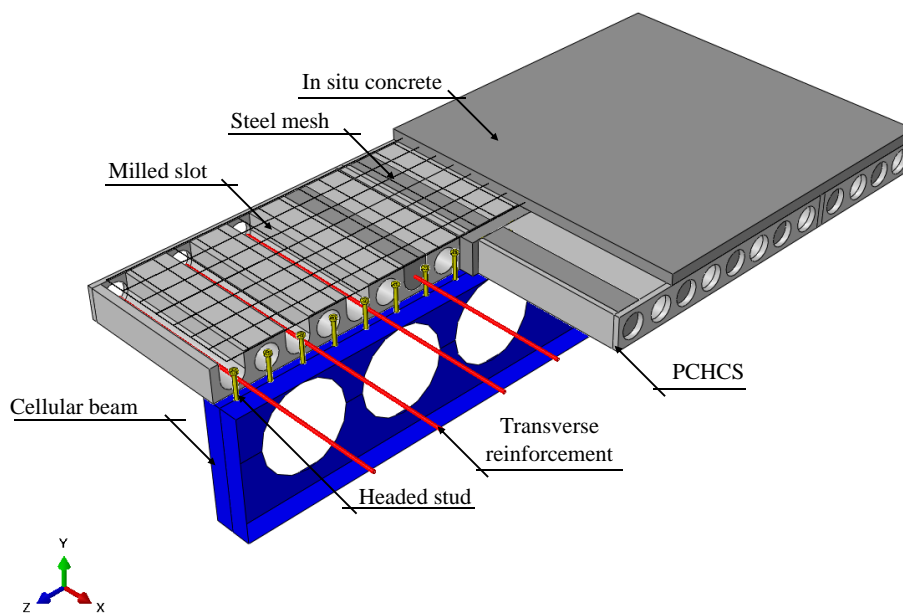
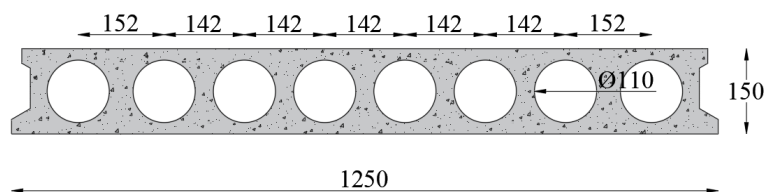


Fig. 10: Finite element model of composite cellular beam with precast hollow core slab and concrete topping

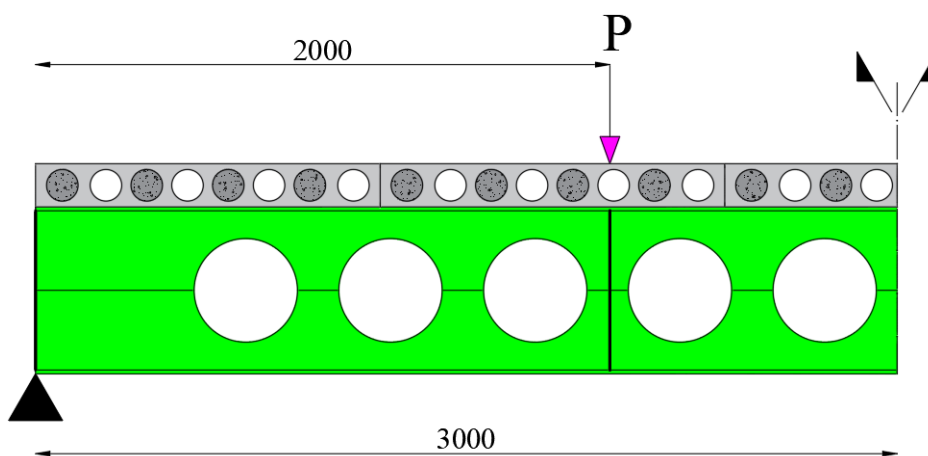
The following are the general considerations for the development of the parametric study:

- i. Steel-concrete composite cellular beams are processed in two steps: Buckle and Static Riks analyses. The initial geometric imperfection factor was applied by a scale factor equal to $dg/1000$ [7];
- ii. The material models are applied according to section 3.2;
- iii. The interaction between parts is applied according to section 3.3;
- iv. Two sections are considered, according **Table 4**;

- 288 v. For each section, three types of slabs are studied: composite beams with Holorib 51/150 geometry, and PCHCS (LP15
 289 units) (**Fig 11**) with and without concrete topping;
- 290 vi. For the cellular profile, ASTM Gr.50 steel is considered, whose yield strength and ultimate strength are 345 MPa and
 291 450 MPa, respectively. The modulus of elasticity and the Poisson's ratio are equal to 200 GPa and 0.3, respectively;
- 292 vii. The infill in situ concrete resistance is 30 MPa, and the PCHCS resistance is 40 MPa;
- 293 viii. For PCHCS, the filling of the 1st, 3rd, 5th and 7th core was considered, and a transversal reinforcement with 16mm of
 294 diameter is placed;
- 295 ix. For PCHCS, 70mm of gap is considered;
- 296 x. The thickness of concrete topping is 50mm, and a steel mesh is 4.2mm spaced at 100mm;
- 297 xi. The dimension of the headed studs is 19x120mm, spaced in 150mm;
- 298 xii. The composite beams are simply supported, according to boundary conditions presented in section 3.4 (**Fig. 5**), with a span
 299 of 6m;
- 300 xiii. The width of the slab is equal to $\frac{1}{4}$ of the span;
- 301 xiv. Four-point bending is considered, and the loads are applied at 2m from the supports. Stiffeners were provided at the points
 302 of loads and supports (**Fig. 12**).



303
304 **Fig. 11: LP 15**



305
306 **Fig. 12: Four-point bending for parametric study**
307
308
309

Table 4: Cellular sections

Sections (Upper/Lower)	d_g	D_o/d	p/D_o	D_o	p	$i/2$
IPE 400 and IPE 400/HEB 340	580	0.8	1.2	320	384	7
		0.8	1.3	320	416	7
		0.8	1.4	320	448	6
		0.8	1.5	320	480	6
		0.9	1.2	360	432	6
		0.9	1.3	360	468	6
		0.9	1.4	360	504	5
		0.9	1.5	360	540	5
		1.0	1.2	400	480	6
		1.0	1.3	400	520	5
		1.0	1.4	400	560	5
		1.0	1.5	400	600	4
		1.1	1.2	440	528	5
		1.1	1.3	440	572	5
		1.1	1.4	440	616	4
		1.1	1.5	440	660	4
		1.2	1.2	480	576	5
		1.2	1.3	480	624	4
		1.2	1.4	480	672	4
		1.2	1.5	480	720	4

5. RESULTS AND DISCUSSION

A total of 120 analyses were carried out. Four failure modes were observed: web post buckling (WPB), web post buckling combined with plastic mechanism (WPB+PM), plastic mechanism (PM), and Vierendeel mechanism (VM). Except for WPB, for other failure modes, shear connector rupture was also observed. The results are discussed with emphasis on the composite cellular beam with PCHCS. At the end of the discussion, a comparative analysis is carried out to assess the ultimate strength depending on the type of slab.

5.1. SYMMETRIC SECTION

Regarding composite cellular beams with composite slabs, the predominant failure mode was WPB, although the WPB+PM and VM, with or without rupture of the shear connectors were also observed. To describe the behavior of these beams step by step, three points of displacement were monitored, considering the mid-span vertical displacement at 10mm, 20mm and the ultimate. In this scenario, the ultimate mid-span vertical displacement showed an average value of approximately 30mm.

The WPB was observed at models $D_o/d=0.8-1.1$, considering $p/D_o=1.2-1.5$. In this scenario, considering the mid-span vertical displacement at 10mm, the magnitude of the global shear force was 183.1 ± 27.6 kN. The shear connectors had already reached the yield strength, with the value of von Mises stresses at 500 ± 16.8 MPa. The lower tee was also reached the yield strength, with von Mises stress values at 345 ± 2.7 MPa. The upper tee, on the other hand, although it was reached the yield strength ($D_o/d=0.8$;

$p/D_o=1.2-1.4$, $D_o/d=0.9$; $p/D_o=1.2-1.3$, $D_o/d=1.0$; $p/D_o=1.2-1.4$, $D_o/d=1.1$; $p/D_o=1.2-1.3$, and $D_o/d=1.2$; $p/D_o=1.2-1.5$, the maximum value of von Mises stresses were 335 ± 18.4 MPa. The openings close to the support, as well as the web posts were in yielding. In this context, considering the composite slab, the lower part of the ribs, which were in the shear region, were damaged by tension. This means that the stresses had already reached the tensile strength of the concrete, as shown in Eq. (2). The upper part of the composite slab, close to the support, was damaged. The concrete compression stresses were 8.1 ± 0.9 MPa. With the progression of loading, for the mid-span vertical displacement prescribed at 20mm, there was a considerable increase in the magnitude of the global shear force in relation to the previous prescribed displacement (10mm), that is, the value of global shear force was 295.3 ± 59.5 kN. Also, there was an increase in plastic deformations, both in the shear connectors and in the upper and lower tees. The maximum von Mises stresses were equal to 489 ± 6 MPa and 353 ± 8 MPa, for the shear connectors and the tees, respectively. Note that in this step, the stress level was lower than the previous situation. This is due to the shear flow between the shear connectors. The damage extended to the side edges of the slab. At this stage, the compressive stresses in the concrete were 13.9 ± 2.4 MPa. Finally, considering the ultimate behavior, the global shear force reached 322.1 ± 61.1 kN. The von Mises stresses for the shear connectors, upper and lower tees were equal to 520 ± 38.2 MPa, 387 ± 32.6 MPa and 389 ± 32.4 MPa, respectively, and the compressive stresses in the concrete were 16.7 ± 2.4 MPa. For models $D_o/d=1.0$; $p/D_o=1.5$ and $D_o=1.1$; $p/D_o=1.4-1.5$, the combination of WPB+PM was observed. During analysis, the behavior of the composite cellular beam was similar to that previously described. However, there was the formation of the plastic mechanism at the upper part of the opening, close to the support. For the series $D_o/d=1.2$, the failure modes observed were WPB ($p/D_o=1.2$), WPB+PM ($p/D_o=1.3$) and VM, with ($p/D_o=1.4$) or without rupture ($p/D_o=1.5$) of the shear connector. The VM, with or without rupture of the shear connector, depending on the longer width of the web post, providing greater resistance to the horizontal shearing force, which causes the Vierendeel moment. Another observation was that with the variation of the web post width, the shear connector rupture was observed. This means that it is not only the axial strengths of the slab and the lower tee that dictate the degree of interaction, but also the spacing between the openings. Next, in Fig. 13, the shear resistance values of the models are shown as a function of the key parameters, for the composite cellular beams with composite slab. It can be seen in the illustration that the lower the D_o/d ratio, the greater the shear resistance. On the other hand, there was no pattern with the variation of the p/D_o ratio, since the end post width was variable and influenced the resistance of composite cellular beams [7].

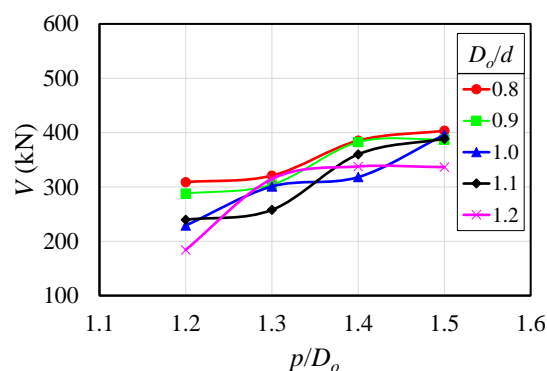
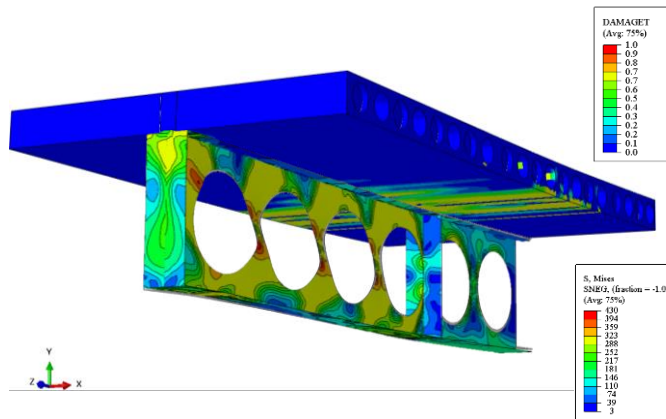
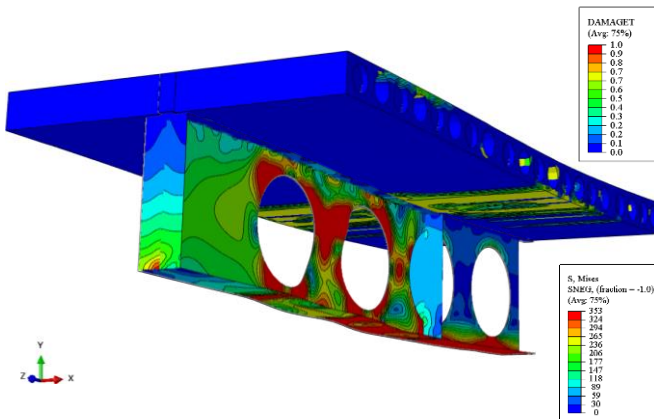


Fig. 13: Global shear force vs. key parameters for symmetric composite cellular beams with composite slab

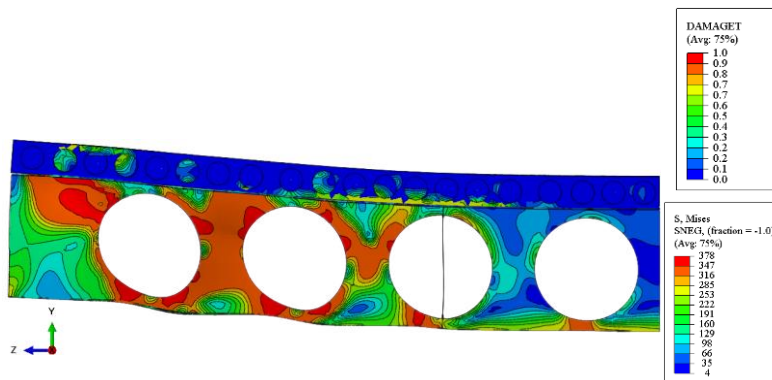
354 Considering the composite cellular beam with hollow core slabs, the failure modes were similar to the models discussed
 355 previously. The failure modes observed were WPB (Fig. 14), the WPB+PM (Fig. 15) and the VM (Fig. 16). In the models, no shear
 356 connector rupture was observed.



357
 358 **Fig. 14: Web post buckling for $D_o/d=1.0$; $p/D_o=1.2$ model, considering PCHCS and symmetrical section**



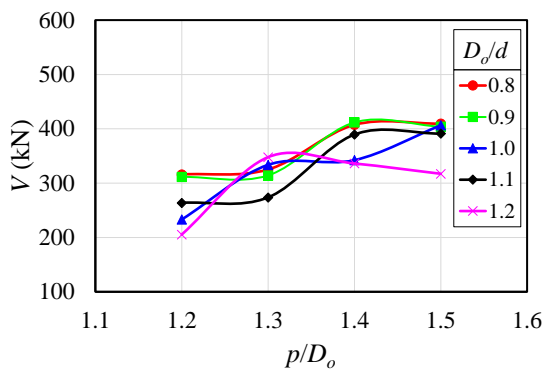
359
 360 **Fig. 15: Web post buckling combined with plastic mechanism for $D_o/d=1.1$; $p/D_o=1.4$ model, considering PCHCS and**
 361 **symmetrical section**



362
 363 **Fig. 16: Vierendeel mechanism without shear connector rupture for $D_o/d=1.1$; $p/D_o=1.4$ model, considering PCHCS and**
 364 **symmetrical section**

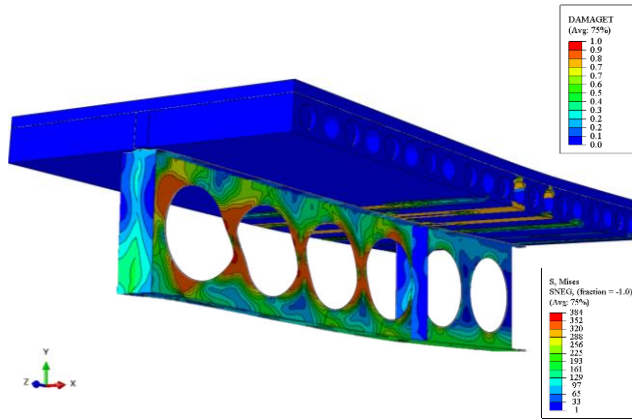
365 For models $D_o/d=0.8-1.1$, considering $p/D_o=1.2-1.5$, the ultimate behavior was governed by WPB. In this scenario,
 366 considering the mid-span vertical displacement at 10mm, the magnitude of global shear load was 186.5 ± 25.9 kN. The shear
 367 connectors had already reached the yield strength. The maximum von Mises stresses in the shear connectors, upper and lower tees

368 were 472 ± 10.8 MPa, 325 ± 21.4 MPa and 344 ± 5.9 MPa, respectively. The openings near the support, as well as the web posts were
 369 also reached the yield strength. In this context, considering the PCHCS, the bottom edge, the gap and the unfilled core close to the
 370 region of the loading application point were damaged by tension. This means that the stresses had already reached the tensile
 371 strength. The upper part of the PCHCS was also damaged. At this stage, the concrete compressive stress was 10.2 ± 0.9 MPa. With
 372 the progression of loading, considering the mid-span vertical displacement at 20mm, the global shear load presented values at
 373 312.4 ± 54.2 kN. There was an increase in plastic deformations, both in the shear connectors and in the upper and lower tees. The
 374 maximum von Mises stresses were 494 ± 11.8 MPa, 352 ± 6.4 MPa and 494 ± 11.82 MPa, for the shear connectors, upper and lower
 375 tees, respectively. In relation to the PCHCS, with the progression of loading, the damage extended to the ends of the slab, increasing
 376 the damaged region. The concrete compressive stresses were 18.7 ± 2.9 MPa. Regarding the ultimate behavior, the values of global
 377 shear force reached, approximately, 337.0 ± 59.4 kN. The von Mises stresses for the shear connectors, upper and lower tees were
 378 518 ± 14.5 MPa, 376 ± 26.4 MPa and 381 ± 29.8 MPa, respectively. In the ultimate strength, the damage by tension spread over the
 379 entire slab, and the concrete compressive stresses reached 23.0 ± 4.7 MPa, and low slip values (almost null) were found at the steel-
 380 concrete interface. On the other hand, for the series $D_o/d=1.2$ with $p/D_o=1.3; 1.5$, WPB+PM was verified (**Fig. 10**), and for the model
 381 $p/D_o=1.4$, the VM was observed (**Fig. 16**). The analysis was processed in a similar way to that previously described. Next, in **Fig. 17**,
 382 the global shear resistance values of the models are shown as a function of the key parameters, considering composite cellular beams
 383 with PCHCS.



384
 385 **Fig. 17: Global shear force vs. key parameters for symmetric composite cellular beams, considering PCHCS and**
 386 **symmetrical section**

387 In relation to the composite cellular beams with PCHCS and concrete topping, WPB (**Fig. 18**) was observed for most
 388 models. The WPB+PM (**Fig. 19**), PM, i.e., plastification of the lower flange or around the opening (**Fig. 20**), and VM (**Fig. 21**),
 389 also occurred.



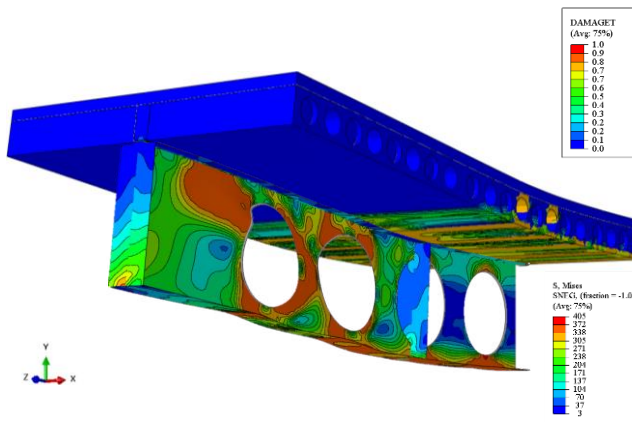
390

391

Fig. 18: Web post buckling for $D_o/d=1.0$; $p/D_o=1.2$ model, considering PCHCS with concrete topping and symmetrical

392

section



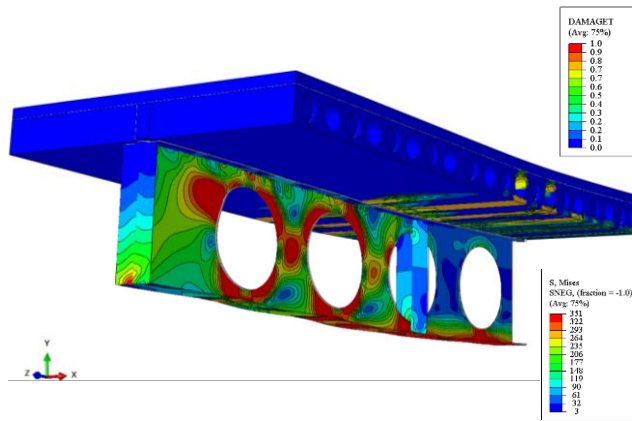
393

394

Fig. 19: Web post buckling combined with plastic mechanism for $D_o/d=1.1$; $p/D_o=1.4$ model, considering PCHCS with

395

concrete topping and symmetrical section



396

397

Fig. 20: Mechanism plastic for $D_o/d=1.1$; $p/D_o=1.5$ model, considering PCHCS with concrete topping and symmetrical

398

section

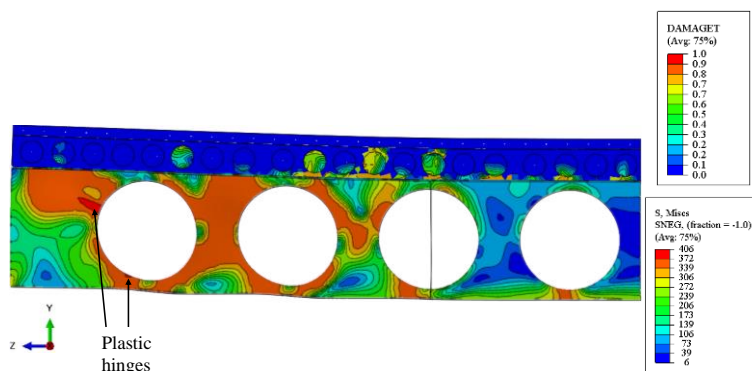


Fig. 21: Vierendeel mechanism for $D_o/d=1.1$; $p/D_o=1.4$ model, considering PCHCS with concrete topping and symmetrical section

For $D_o/d=0.8$; $p/D_o=1.2-1.5$, $D_o/d=0.9$; $p/D_o=1.2-1.5$, $D_o/d=1.0$; $p/D_o=1.2-1.4$, $D_o/d=1.1$; $p/D_o=1.2-1.3$ and $D_o/d=1.2$; $p/D_o=1.2$ models, the ultimate behavior was governed by WPB. Regarding the processing of the models, considering the mid-span vertical displacement at 10mm, the magnitude of global shear force was 231.5 ± 28.8 kN. The shear connectors had already reached the yield strength, with the maximum von Mises stresses of 401 ± 4.3 MPa. In this scenario, the von Mises stresses in the upper and lower tees were 334 ± 14.5 MPa and 346 ± 6.4 MPa, respectively. The openings and web posts, in the region of pure shear, were already in plastification. In this context of prescribed displacement, the elements of the PCHCS, such as the lower edge, the gap, the core without filling, were damaged. For situations in which the end post width is much greater than the web post width, damage was also verified in the upper part of the concrete topping, close to the support, where the shear is maximum. In this scenario, the concrete compressive stresses were 8.7 ± 2.8 MPa. With the progression of loading, for the mid-span vertical displacement prescribed at 20mm, the global shear force presented values at 368.8 ± 55.9 kN. There was an increase in plastic deformations, both in the shear connectors and in the upper and lower tees. In this context, the maximum von Mises stresses for the shear and tees connectors were 522 ± 15.3 MPa and 354 ± 9 MPa, respectively. In the PCHCS with concrete topping, there was an increase in the damaged region. The concrete compressive stresses were 16.8 ± 5.3 MPa. In the ultimate strength, the magnitude of global shear force reached 383.1 ± 65.3 kN. The von Mises stresses for the shear connectors, upper and lower tees were 557 ± 33 MPa, 371 ± 23.1 MPa and 378 ± 30 MPa, respectively. In this scenario, considering the PCHCS, there was an increase in the damaged region, that is, excessive cracking, and the concrete compressive stresses reached 17.8 ± 4.6 MPa. Also, low slip values were verified at the steel-concrete interface. An important observation was the contribution of the concrete topping, which it maintained as compression stresses below, in comparison with the PCHCS models. For the situations that occurred WPB+PM ($D_o/d=1.0$; $p/D_o=1.5$ and $D_o/d=1.5$; $p/D_o=1.0$), PM ($D_o/d=1.1$; $p/D_o=1.4-1.5$ and $D_o/d=1.2$; $p/D_o=1.3$) and VM ($D_o/d=1.2$; $p/D_o=1.4$), a higher loading was observed, as well as plastic deformations. This occurred due to the end and web posts widths. **Fig. 22** illustrates the shear resistance values of the models as a function of the key parameters, considering composite cellular beams with PCHCS and concrete topping.

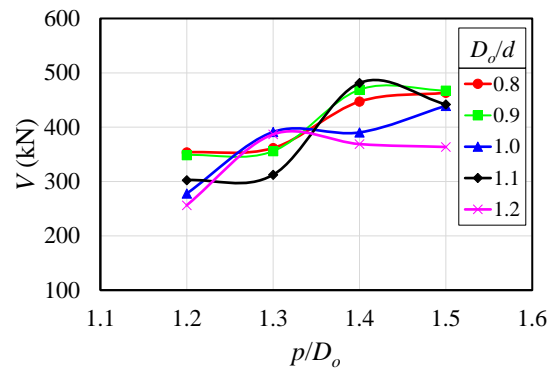


Fig. 22: Global shear force vs. key parameters for symmetric composite cellular beams, considering PCHCS with concrete topping and symmetrical section

5.2. ASYMMETRIC SECTION

Regarding the structural behavior of asymmetric composite cellular beams with composite slabs, the failure modes were WPB+PM, PM and VM, with or without shear connector rupture. Also, three points of mid-span vertical displacement were monitored to describe the structural behavior. The monitored points were 10mm, 20mm and 41.4±14mm.

The failure mode WPB+PM was observed for $D_o/d=0.8$; $p/D_o=1.2-1.3$ and 1.5, $D_o/d=0.9$; $p/D_o=1.2-1.5$, $D_o/d=1.0$; $p/D_o=1.2-1.5$, $D_o/d=1.1$; $p/D_o=1.2-1.5$ and $D_o/d=1.2$; $p/D_o=1.2-1.3$. In this scenario, the shear connector rupture was observed for $D_o/d=0.8$; $p/D_o=1.2$, $D_o/d=0.9$; $p/D_o=1.2$, $D_o/d=1.0$; $p/D_o=1.2$, and $D_o/d=1.2$; $p/D_o=1.2$. Regarding the structural behavior during the analysis, and considering the mid-span vertical displacement at 10mm, the global shear force presented values at 265.4±49.2 kN. The shear connectors had already reached the yield strength. The von Mises stresses in the shear connectors were 490±11.1 MPa. The upper and lower tees were also already in plastic regime, with von Mises stresses of 347±0.7 MPa, for both the lower and upper tees. The openings close to the support (shear region), as well as the web posts were also in a plastic regime. On the behavior of the composite slab, with the mid-span vertical displacement prescribed at 10mm, the lower part of the ribs that were in the shear region were damaged. For situations where the end-post was much larger than the web post, the upper part of the slab, which was close to the support, was damaged. At this stage, the concrete compressive stresses were 11.2±1.6 MPa. With the progression of loading, in which the global shear force was 373.9±75.6 kN and the mid-span vertical displacement at 20mm, there was an increase in plastic deformations, both in the shear connectors, and in the upper and lower tees. In this context, maximum von Mises stresses were 509±23 MPa and 361±9.9 MPa, for shear connectors and tees, respectively. In relation to the composite slab, there was an increase in the damaged region, and the concrete compressive stresses were 18.0±3.1 MPa. In the ultimate behavior, the global shear force reached 440.3±77.4 kN. The von Mises stresses for the shear connectors, upper and lower tees were 625±40.2 MPa, 435±46.6 MPa and 407±42.4 MPa, respectively. In this scenario, in the composite slab there was an increase in the damaged region, that was, the cracks extended from the lower part of the rib to the mid-height of the slab, and the compressive stresses of the concrete were measured in 24.5±3.0 MPa. In addition, there were low slip values at the steel-concrete interface. Oppositely, for $D_o/d=0.8$; $p/D_o=1.4$

and $D_o/d=1.2$; $p/D_o=1.4-1.5$, the formation of the plastic mechanism and the Vierendeel mechanism were observed, respectively.

Fig. 23 illustrates the resistance values, considering the global shear in function of the key parameters.

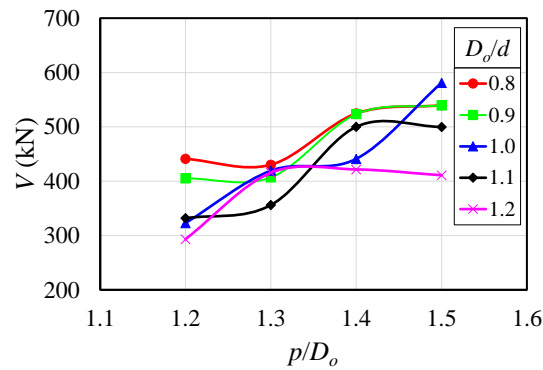
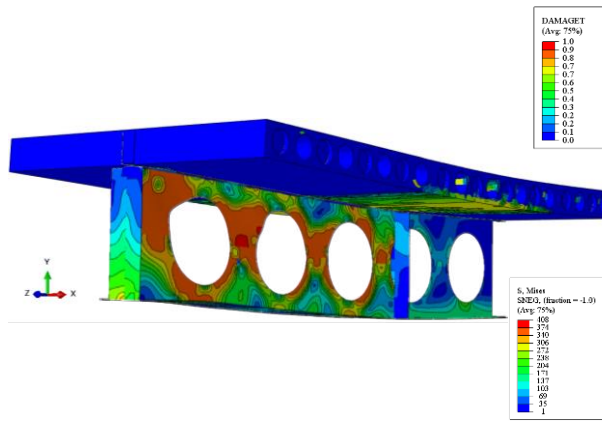


Fig. 23: Global shear force vs. key parameters for asymmetric composite cellular beams with composite slab

With regard to asymmetric composite cellular beams with PCHCS, the predominant failure modes were WPB+PM (**Fig. 24**). Only the $D_o/d=1.2$; $p/D_o=1.5$ model presented the plastic mechanism (**Fig. 25**), without buckling. For $D_o/d=0.8$; $p/D_o=1.2-1.3$ and 1.5 , $D_o/d=0.9-1.1$; $p/D_o=1.2$, the shear connector rupture was observed. Considering the structural behavior of asymmetric composite cellular beams with PCHCS, for the mid-span vertical displacement prescribed at 10mm, the global shear force presented was 272 ± 44.9 kN. The shear connectors had already reached the yield strength. The maximum stresses of von Mises were 482 ± 7.4 MPa. In this scenario, the von Mises stresses in the tees were 346 ± 0.7 MPa. The openings and web posts, which were close to the support, had already reached the yield strength. For the mid-span vertical displacement prescribed at 10mm, the bottom edge of the PCHCS, the gap and the unfilled core, close to the region of the loading application point, were damaged. The upper part of the PCHCS was also damaged. In this scenario, the concrete compressive stresses were 14.6 ± 1.8 MPa. With the progression of loading, for the mid-span vertical displacement prescribed at 20mm, the global shear force was 391.5 ± 72.7 kN. There was an increase in plastic deformations, both in the shear connectors and in the tees. In this context, the maximum von Mises stresses were 516 ± 17.3 MPa and 357 ± 6.1 MPa, for the shear connectors and the tees, respectively. In this scenario, the damage extended to the sides of the PCHCS. At this stage the compressive stresses were 25.2 ± 4.5 MPa. In the ultimate behavior, for mid-span vertical displacement prescribed at 49.7 ± 21.8 mm, the global shear load and the concrete compressive stresses reached 469.7 ± 71.1 kN and 30.3 ± 6.0 MPa, respectively. The von Mises stresses for the shear connectors, upper and lower tees were 617 ± 44.1 MPa, 434 ± 36.9 MPa and 420 ± 52.1 MPa, respectively. In addition, low slip values (null) were also found at the steel-concrete interface. **Fig. 26** illustrates the shear resistance values of the models as a function of the key parameters, considering asymmetric composite cellular beams with PCHCS.

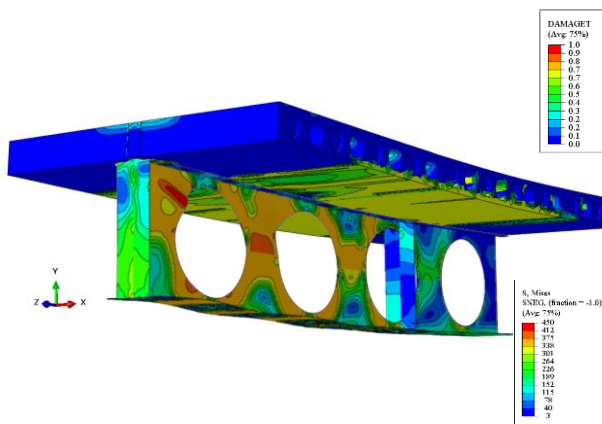


470

471

472

Fig. 24: Web post buckling combined with plastic mechanism for $D_o/d=1.0$; $p/D_o=1.4$ model, considering PCHCS and asymmetrical section

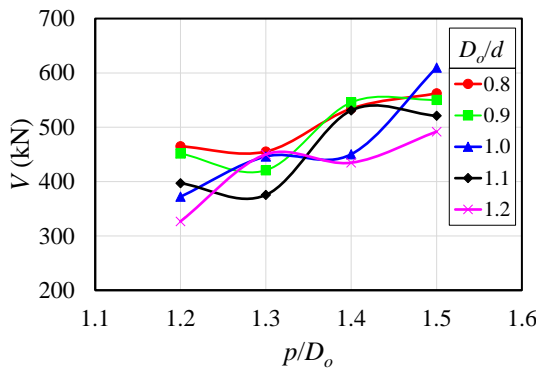


473

474

475

Fig. 25: Plastic mechanism for $D_o/d=1.2$; $p/D_o=1.5$ model, considering and asymmetrical section



476

477

Fig. 26: Global shear force vs. key parameters for asymmetric composite cellular beams, considering PCHCS

478

479

480

481

482

With regard to the asymmetrical composite cellular beams with PCHCS and concrete topping, the failure modes observed were WPB+PM (Fig. 27), for $D_o/d=0.8$; $p/D_o=1.1$, $D_o/d=0.9$; $p/D_o=1.2-1.3$, $D_o/d=1.0$; $p/D_o=1.2-1.4$, $D_o/d=1.1$; $p/D_o=1.2-1.3$ and $D_o/d=1.2$; $p/D_o=1.2-1.3$, and PM (Fig. 28), for $D_o/d=0.8$; $p/D_o=1.3-1.5$, $D_o/d=0.9$; $p/D_o=1.4-1.5$, $D_o/d=1.0$; $p/D_o=1.5$, $D_o/d=1.1$; $p/D_o=1.4-1.5$ and $D_o/d=1.2$; $p/D_o=1.4-1.5$. In this scenario, there was no shear connector rupture for only $D_o/d=1.1-1.2$; $p/D_o=1.3$ models. Regarding the structural behavior analyzed, considering the mid-span vertical displacement prescribed at 10 mm, the global

shear force was 331.4 ± 50.6 kN. The shear connectors and the tees had already reached the yield strength, with von Mises stresses of 488 ± 8.1 MPa and 347 ± 0.9 MPa, respectively. At this stage, the bottom edge of the PCHCS, the gap and the unfilled core near the region of the loading application point were damaged. The upper part of the concrete topping, next to the support, was also damaged. The concrete compressive stresses were 12.3 ± 3.7 MPa. This was also verified for the previous situations, in which the end post width was greater than the web post width. With the progression of loading, for the mid-span vertical displacement at 20mm, the global shear load was 448.3 ± 82.7 kN. There was an increase in plastic deformations in the shear and tees connectors. In this context, the maximum von Mises stresses were 557 ± 28.3 MPa and 362 ± 9.2 MPa, for the shear connectors and the tees, respectively. Considering the PCHCS with concrete topping, the damage extended to the side edges. The concrete compressive stresses were 20.4 ± 6.5 MPa. In the ultimate behavior, for the mid-span vertical displacement prescribed at 37.3 ± 8.6 mm, the magnitude of global shear reached 513.3 ± 71.2 kN. The von Mises stresses for the shear connectors, upper and lower tees were 659 ± 11.9 MPa, 437 ± 16.9 MPa and 414 ± 29.4 MPa. The concrete compressive stresses were 20.0 ± 4.6 MPa and, in most models, the shear connector rupture was observed. In addition, there were low slip values at the steel-concrete interface. **Fig. 29** illustrates the shear resistance values of the models as a function of the key parameters, considering asymmetric composite cellular beams with PCHCS and concrete topping.

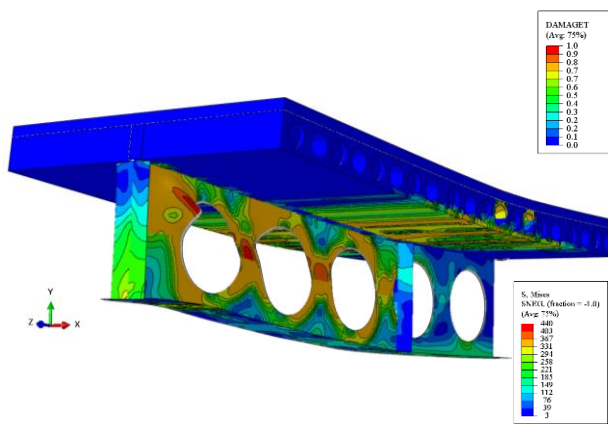
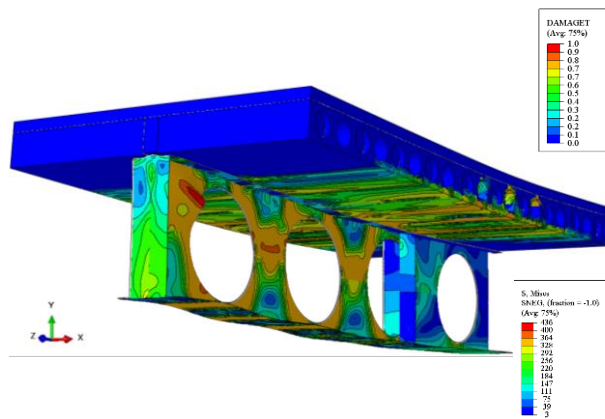
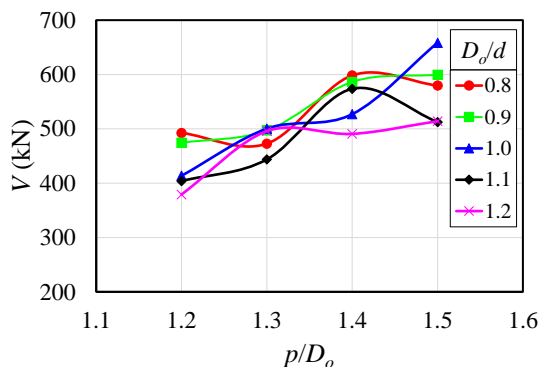


Fig. 27: Web post buckling combined with plastic mechanism for $D_o/d=1.0$; $p/D_o=1.4$ model, considering PCHCS with concrete topping and asymmetrical section



498
499
500
501

502 **Fig. 28: Plastic mechanism for $D_o/d=1.2$; $p/D_o=1.5$ model, considering PCHCS with concrete topping and asymmetrical**
 503 **section**



504 **Fig. 29: Global shear force vs. key parameters for asymmetrical composite cellular beams, considering PCHCS with**
 505 **concrete topping and asymmetrical section**

507 5.3. COMPARATIVE ANALYSIS BETWEEN MODELS

508 In the previous sections, the behavior of composite cellular beams, considering composite slabs, PCHCS, and PCHCS with
 509 concrete topping were discussed. In this section, the shear resistance is discussed through comparative analyses. In **Fig. 30**, the
 510 results are illustrated considering the symmetric section. As shown in **Fig. 30a**, considering $D_o/d=0.8$, a situation in which the
 511 highest depth of the tee sections was found, the maximum differences between the PCHCS and the composite slab models ($V_{PCHCS}-$
 512 V_{CS}), PCHCS with concrete topping and composite slab models ($V_{PCHCSCT}-V_{CS}$), and PCHCS with concrete topping and PCHCS
 513 ($V_{PCHCSCT}-V_{PCHCS}$) were 22kN, 62 kN and 54 kN, respectively. These values were measured for $p/D_o=1.4-1.5$ and $b_{we}/b_w=1.3-2.9$. In
 514 these cases, it was observed that the PCHCS models obtained greater resistance when compared to the composite slab, for situations
 515 in which the ultimate strength was reached by WPB. This means that the slab contributed significantly to the strength of the
 516 composite cellular beams. For $D_o/d=0.9$ (**Fig. 30b**), the maximum differences between the resistance values were $V_{PCHCS}-V_{CS}=29$ kN
 517 ($p/D_o=1.4$ and $b_{we}/b_w=3.8$), $V_{PCHCSCT}-V_{CS}=86$ kN ($p/D_o=1.4$ and $b_{we}/b_w=3.8$), and $V_{PCHCSCT}-V_{PCHCS}=64$ kN ($p/D_o=1.5$ and $b_{we}/b_w=2.2$).
 518 Although in the present situation the depth of the tee sections decreased with increasing diameter, with increasing diameter the web
 519 post width was increased. Thus, when compared to the previous situation, the differences between the types of slab increased,
 520 showing the influence of the web posts width on the shear resistance. Considering $D_o/d=1.0$ (**Fig. 30c**), the maximum differences
 521 were measured for $p/D_o=1.3$. The values obtained were $V_{PCHCS}-V_{CS}=33$ kN, $V_{PCHCSCT}-V_{CS}=90$ kN and $V_{PCHCSCT}-V_{PCHCS}=57$ kN. For
 522 these situations, WPB was observed. For $D_o/d=1.1$ (**Fig. 30d**), the maximum differences between the PCHCS and composite slab
 523 ($V_{PCHCS}-V_{CS}$), PCHCS with concrete topping and composite slab ($V_{PCHCSCT}-V_{CS}$), and PCHCS with concrete topping and PCHCS
 524 ($V_{PCHCSCT}-V_{PCHCS}$) were 29kN, 121 kN and 92 kN, respectively. These values were measured for $p/D_o=1.4$ and $b_{we}/b_w=3.5$. In this
 525 case, it was observed that as the opening diameter was increased, the difference between the PCHCS and composite slab was
 526 decreased. However, the differences between these two types of slab, when compared to the PCHCS with concrete topping, tend to
 527 increase. Finally, considering $D_o/d=1.2$, (**Fig. 30e**), for the situation that WPB occurred ($p/D_o=1.2$), the differences were $V_{PCHCS}-$

528 $V_{CS}=21\text{kN}$, $V_{PCHCSCT}-V_{CS}=72\text{kN}$ e $V_{PCHCSCT}-V_{PCHCS}=51\text{kN}$. For the other situations in which some plastic behavior was observed,
 529 such as the VM, the values of the differences decreased, since this ultimate behavior was governed by the yield strength of the tees.
 530 In **Fig. 31**, some examples of these differences are illustrated through the equilibrium trajectory, considering WPB.

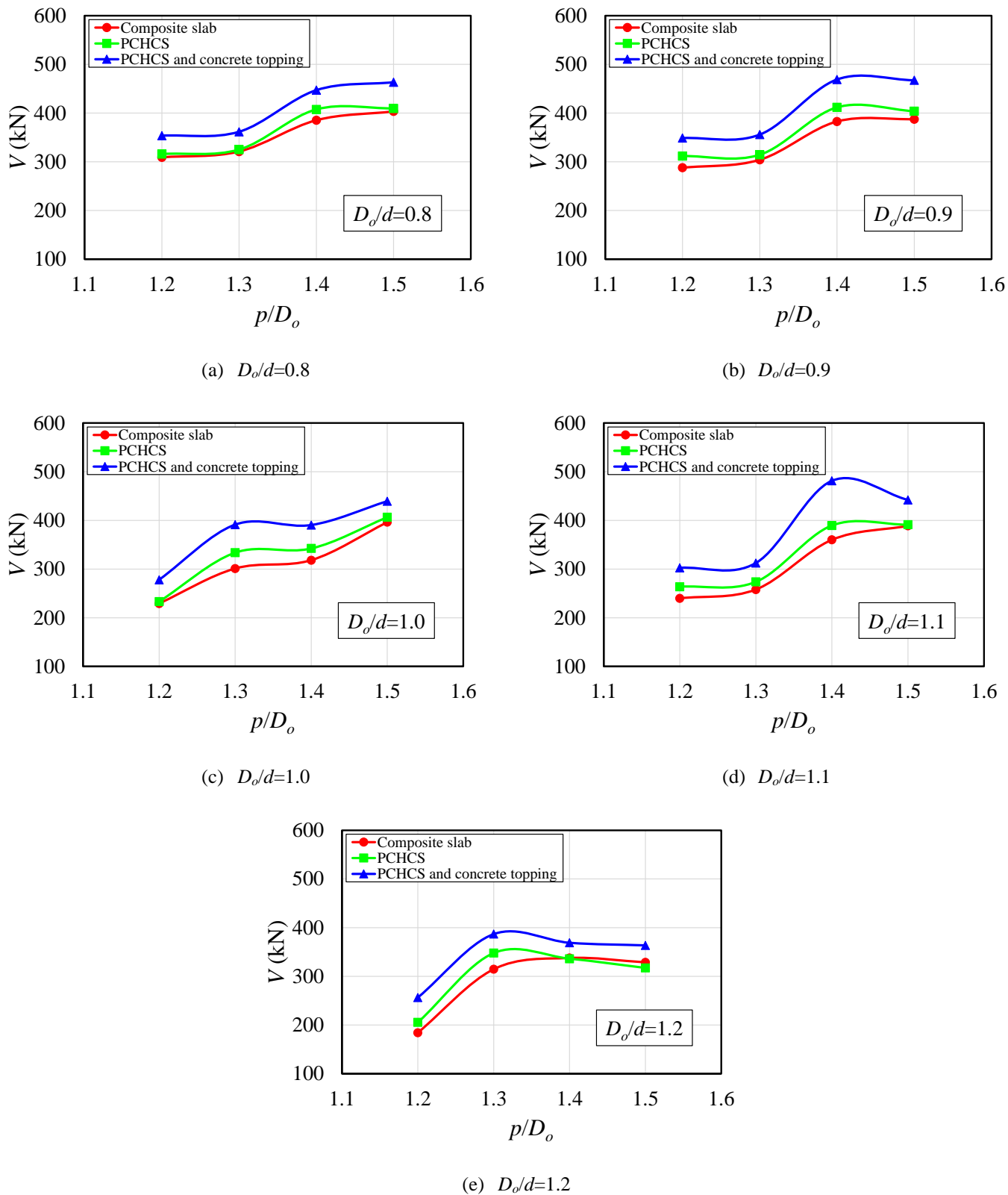
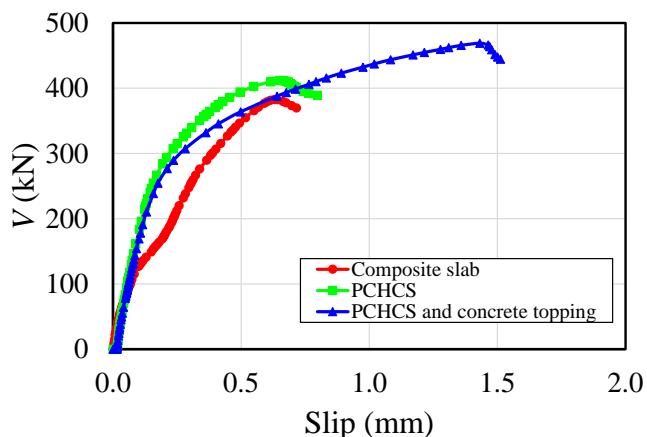
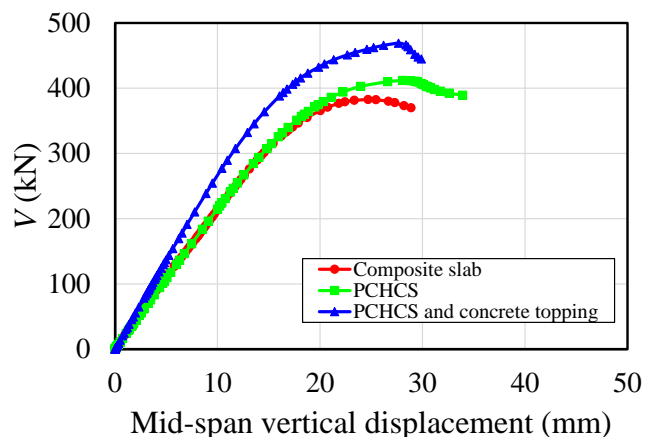
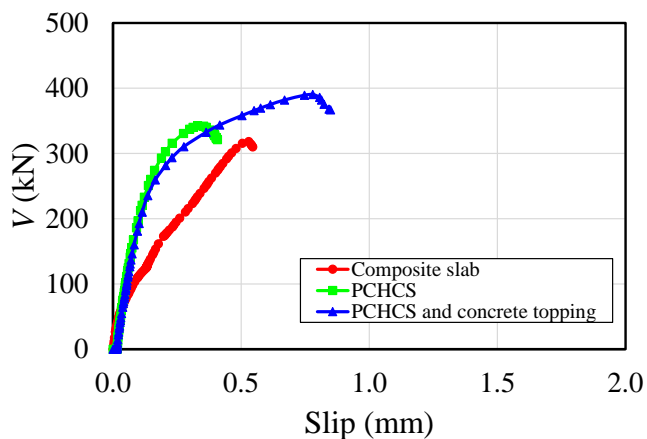
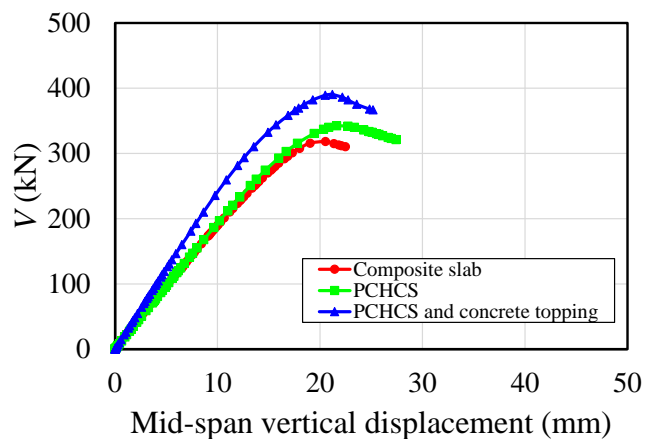
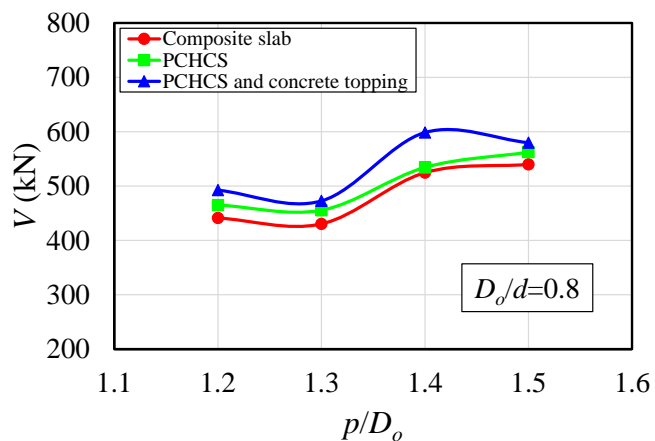
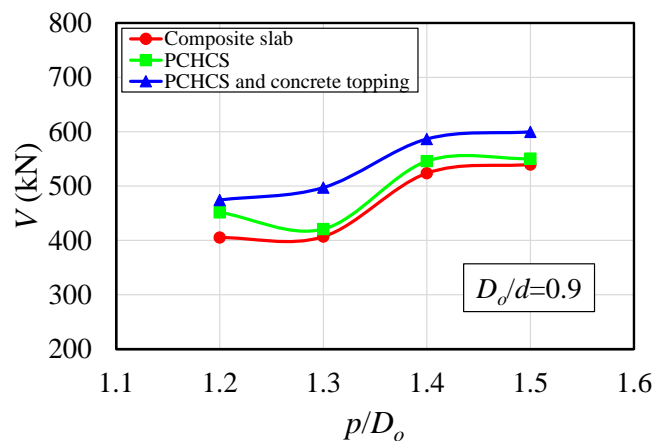
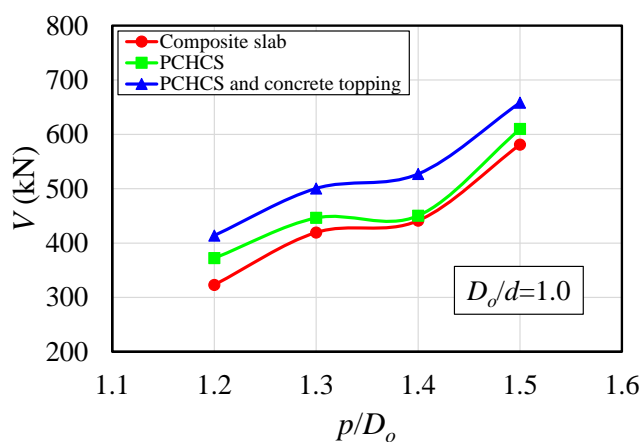
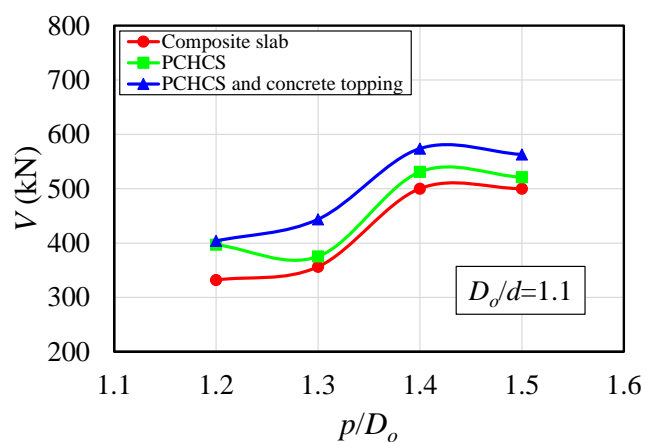
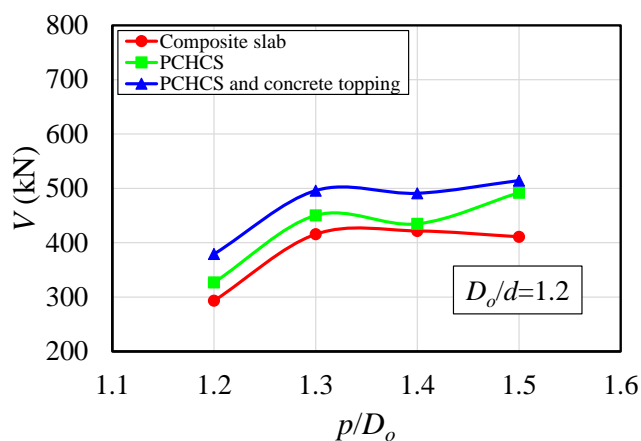


Fig. 30: Comparative analyses for symmetric composite cellular beams

(a) Shear-slip relationship for $D_o/d=0.9$ and $p/D_o=1.4$ (b) Shear-deflection relationship for $D_o/d=0.9$ and $p/D_o=1.4$ (c) Shear-slip relationship for $D_o/d=1.0$ and $p/D_o=1.4$ (d) Shear-deflection relationship for $D_o/d=1.0$ and $p/D_o=1.4$ **Fig. 31: Differences in the behavior of composite cellular beams with slab variation, considering symmetrical section**

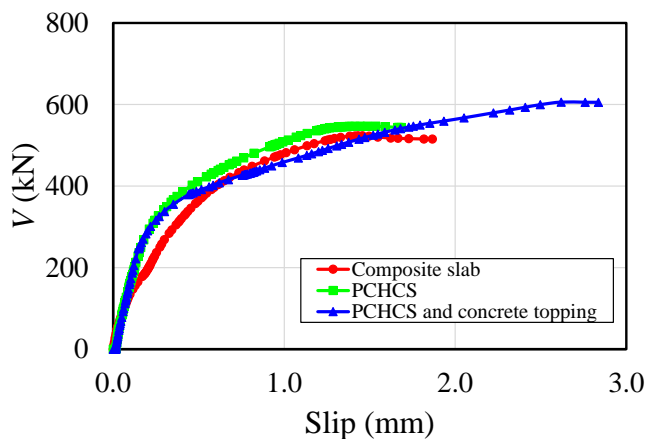
On the other hand, **Fig. 32** illustrates the results for asymmetric section. Considering $D_o/d=0.8$ (**Fig. 32a**), the maximum differences were $V_{PCHCS}-V_{CS}=25\text{kN}$, $V_{PCHCSCT}-V_{CS}=74\text{kN}$ and $V_{PCHCSCT}-V_{PCHCS}=64\text{kN}$. These values were measured for $p/D_o=1.3-1.4$ and $b_{we}/b_w=1.3-2.9$. For $D_o/d=0.9$ (**Fig. 32b**), the maximum differences between the resistance values were $V_{PCHCS}-V_{CS}=46\text{kN}$ ($p/D_o=1.2$ and $b_{we}/b_w=6.2$), $V_{PCHCSCT}-V_{CS}=90\text{kN}$ ($p/D_o=1.3$ and $b_{we}/b_w=2.3$), and $V_{PCHCSCT}-V_{PCHCS}=76\text{kN}$ ($p/D_o=1.3$ and $b_{we}/b_w=2.3$). Considering $D_o/d=1.0$ (**Fig. 32c**), the maximum differences were measured for $p/D_o=1.2;1.4$. The values obtained were $V_{PCHCS}-V_{CS}=49\text{kN}$ ($p/D_o=1.2$), $V_{PCHCSCT}-V_{CS}=91\text{kN}$ ($p/D_o=1.4$) and $V_{PCHCSCT}-V_{PCHCS}=77\text{kN}$ ($p/D_o=1.4$). For these situations, WPB+PM with shear connector rupture was observed. For $D_o/d=1.1$ (**Fig. 32d**), the maximum differences were $V_{PCHCS}-V_{CS}=65\text{kN}$, $V_{PCHCSCT}-V_{CS}=88\text{kN}$ and $V_{PCHCSCT}-V_{PCHCS}=68\text{kN}$. These values were measured for $p/D_o=1.2-1.3$ and $b_{we}/b_w=1.6-4.6$. Finally, considering $D_o/d=1.2$, (**Fig. 32e**), the differences were $V_{PCHCS}-V_{CS}=81\text{kN}$ ($p/D_o=1.5$), $V_{PCHCSCT}-V_{CS}=103\text{kN}$ ($p/D_o=1.5$) and $V_{PCHCSCT}-V_{PCHCS}=56\text{kN}$ ($p/D_o=1.4$). In **Fig. 33**, some examples of these differences are illustrated through the equilibrium trajectory.

(a) $D_o/d=0.8$ (b) $D_o/d=0.9$ (c) $D_o/d=1.0$ (d) $D_o/d=1.1$ (e) $D_o/d=1.2$

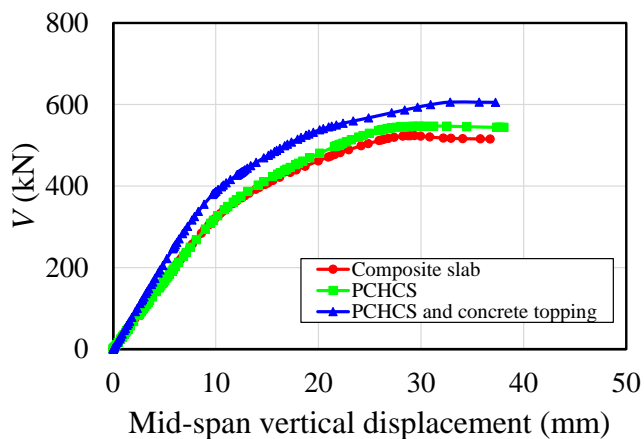
544 **Fig. 32: Comparative analyses for asymmetric composite cellular beams**

545

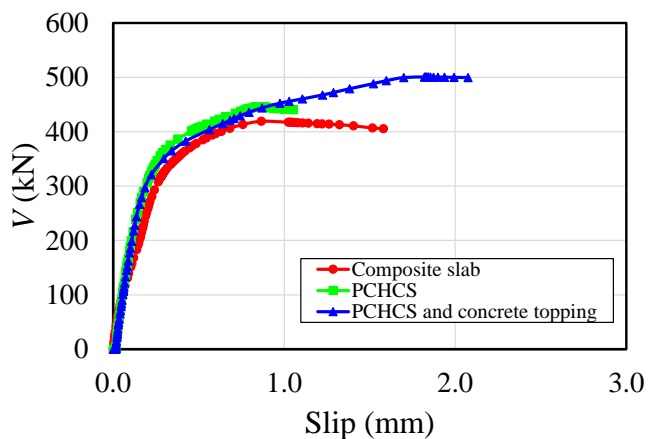
546



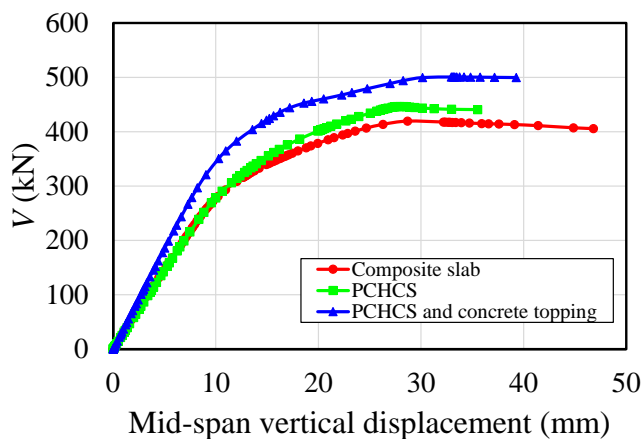
(a) Shear-slip relationship for $D_o/d=0.9$ and $p/D_o=1.4$



(b) Shear-deflection relationship for $D_o/d=0.9$ and $p/D_o=1.4$



(c) Shear-slip relationship for $D_o/d=1.0$ and $p/D_o=1.3$



(d) Shear-deflection relationship for $D_o/d=1.0$ and $p/D_o=1.3$

Fig. 33: Differences in the behavior of composite cellular beams with slab variation, considering asymmetrical section

In general, for composite cellular beams with composite slab and PCHCS, the asymmetric section showed greater efficiency in terms of shear resistance. On the other hand, considering PCHCS with concrete topping, the symmetrical sections showed greater resistance. This was due to the ultimate behavior being governed by shear connector rupture. **Table 5** shows all the results obtained.

547
548
549
550
551
552
553
554
555
556
557
558

559 **Table 5: Summary of numerical results**

D_o/d	p/D_o	b_{wc}/b_w	Symmetric section						Asymmetric section					
			Composite slab		PCHCS		PCHCS and concrete topping		Composite slab		PCHCS		PCHCS and concrete topping	
			V (kN)	Failure	V (kN)	Failure	V (kN)	Failure	V (kN)	Failure	V (kN)	Failure	V (kN)	Failure
0.8	1.2	5.4	309	WPB	316	WPB	354	WPB	441	WPB+PM*	465	WPB+PM*	493	WPB+PM*
	1.3	1.4	321	WPB	325	WPB	362	WPB	430	WPB+PM	455	WPB+PM*	473	PM*
	1.4	2.9	385	WPB	407	WPB	447	WPB	525	PM*	534	WPB+PM	599	PM*
	1.5	1.3	404	WPB	410	WPB	463	WPB	540	WPB+PM	562	WPB+PM*	580	PM*
0.9	1.2	6.2	288	WPB	312	WPB	349	WPB	405	WPB+PM*	452	WPB+PM*	474	WPB+PM*
	1.3	2.3	304	WPB	314	WPB	356	WPB	407	WPB+PM	421	WPB+PM	497	WPB+PM*
	1.4	3.8	383	WPB	412	WPB	469	WPB	524	WPB+PM	546	WPB+PM	586	PM*
	1.5	2.2	387	WPB	404	WPB	467	WPB	540	WPB+PM	550	WPB+PM	600	PM*
1.0	1.2	2.0	229	WPB	233	WPB	278	WPB	323	WPB+PM*	372	WPB+PM*	414	WPB+PM*
	1.3	3.8	301	WPB	334	WPB	391	WPB	419	WPB+PM	446	WPB+PM	501	WPB+PM*
	1.4	1.8	318	WPB	342	WPB	390	WPB	441	WPB+PM	450	WPB+PM	527	WPB+PM*
	1.5	3.5	396	WPB+PM	407	WPB+PM	439	WPB+PM	581	WPB+PM	610	WPB+PM	658	PM*
1.1	1.2	4.6	240	WPB	264	WPB	303	WPB	332	WPB+PM	397	WPB+PM*	404	WPB+PM*
	1.3	1.6	258	WPB	274	WPB	312	WPB	356	WPB+PM	376	WPB+PM	444	WPB+PM
	1.4	3.5	360	WPB+PM	390	WPB+PM	481	PM	500	WPB+PM	531	WPB+PM	574	PM*
	1.5	2.1	389	WPB+PM	391	WPB+PM	442	PM	500	WPB+PM	521	WPB+PM	563	PM*
1.2	1.2	1.8	184	WPB	205	WPB	256	WPB	293	WPB+PM*	327	WPB+PM*	379	WPB+PM*
	1.3	4.0	315	WPB+PM	348	WPB+PM	387	PM	416	WPB+PM	450	WPB+PM	496	WPB+PM
	1.4	2.1	338	VM	336	VM	369	VM	422	VM*	435	WPB+PM	491	PM*
	1.5	1.0	329	VM*	317	WPB+PM	364	WPB+PM	411	VM*	492	PM	514	PM*

*Shear connector rupture was observed

5.4. ULTIMATE STRENGTH OF COMPOSITE CELLULAR BEAMS WITH PCHCS VS. DESIGN RECOMENDATIONS

In this section, the numerical results are compared with the existing analytical procedures. Only the results of composite cellular beams with PCHCS and PCHCSCT are considered, since in Ferreira et al. [7] the WPB resistance of composite cellular beams with composite slab has been investigated. It is worth mentioning that, in the authors' conclusion, it was verified that the existing models underestimate the resistance of composite cellular beams, since the calculation models do not take into account the contribution of the concrete slab in the resistance to WPB.

As presented in section 5.3, the WPB was the predominant failure mode. Although WPB+PM has occurred in some situations, it is considered only the most critical situation, that is, WPB, as presented by Lawson et al. [18]. For this, two calculation recommendations are used: SCI P355 [19] and Steel Design Guide 31 [85], which are based on EC4 [29] and ANSI / AISC 360-16 [86]. For the calculation of the WPB resistance, SCI P355 [19] addresses the compressed bar theory (Eqs. 13-19):

$$\sigma_{Rk} = \chi f_y \quad (13)$$

$$\chi = \frac{1}{\phi + \sqrt{\phi^2 - \bar{\lambda}^2}} \leq 1.0 \quad (14)$$

$$\phi = 0.5 \left[1 + 0.49 (\bar{\lambda} - 0.2) + \bar{\lambda}^2 \right] \quad (15)$$

$$\bar{\lambda} = \sqrt{\frac{f_y}{f_{cr,w}}} \quad (16)$$

$$f_{cr,w} = \frac{\pi^2 E}{\lambda_w^2} \quad (17)$$

$$\lambda_w = \frac{l_{eff} \sqrt{12}}{t_w} \quad (18)$$

$$V_{Rk} = \sigma_{Rk} t_w b_w \quad (19)$$

On the other hand, Steel Design Guide 31 [85] is based on the horizontal shear force that acts on the web post, as shown previously in Fig. 2. For this, it will be necessary to extract the horizontal shear force from the numerical model (Eqs 20-21). This methodology is analogous to that presented in Ferreira et al. [7], as shown in Fig 34.

$$V_{h,FE} = \left| \frac{M_{FE(i+1)} - M_{FE(i)}}{d_{eff}} \right| \quad (20)$$

$$d_{ef,comp} = d_g - y_{o,inf} + 0.5t_c \quad (21)$$

For the case of four-point bending, a situation in which the global shear is constant, **Eq. (20)** can be replaced by **Eq. (22)**.

$$V_{h,FE} = \frac{pV_{FE}}{d_{eff}} \quad (22)$$

$$M_{vh} = 0.9 \left(\frac{D_o}{2} \right) V_h \quad (23)$$

$$M_{w,Rk} = M_{w,e} \left[C1 \left(\frac{p}{D_o} \right) - C2 \left(\frac{p}{D_o} \right)^2 - C3 \right] \quad (24)$$

$$M_{w,e} = \frac{t_w (p - D_o + 0.564 D_o)^2}{6} f_y \quad (25)$$

$$C1 = 5.097 + 0.1464 \left(\frac{D_o}{t_w} \right) - 0.00174 \left(\frac{D_o}{t_w} \right)^2 \quad (26)$$

$$C2 = 1.441 + 0.0625 \left(\frac{D_o}{t_w} \right) - 0.000683 \left(\frac{D_o}{t_w} \right)^2 \quad (27)$$

$$C3 = 3.645 + 0.0853 \left(\frac{D_o}{t_w} \right) - 0.00108 \left(\frac{D_o}{t_w} \right)^2 \quad (28)$$

$$V_{h,Rk} = \frac{M_{w,e}}{0.45 D_o} \left[C1 \left(\frac{p}{D_o} \right) - C2 \left(\frac{p}{D_o} \right)^2 - C3 \right] \quad (29)$$

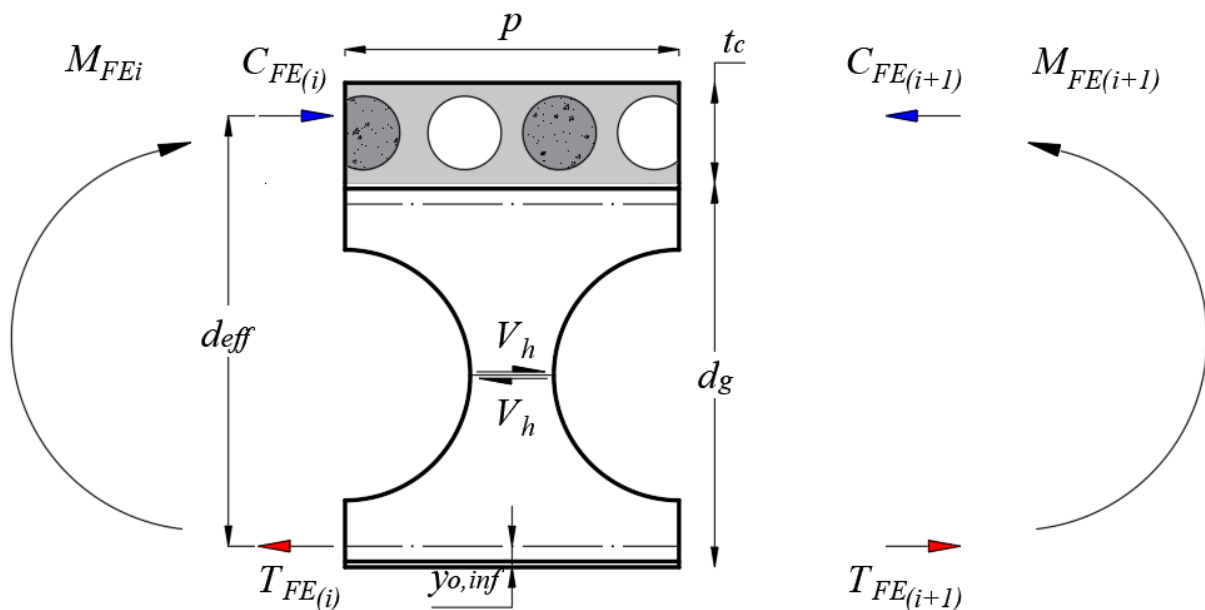
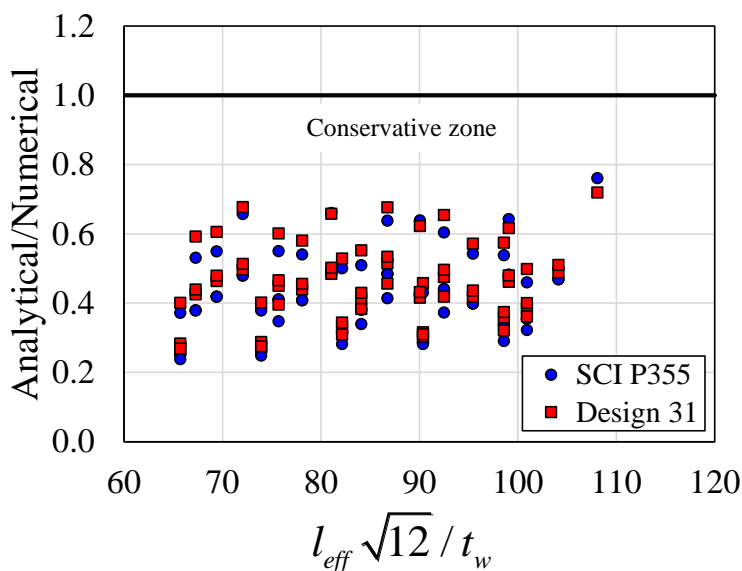
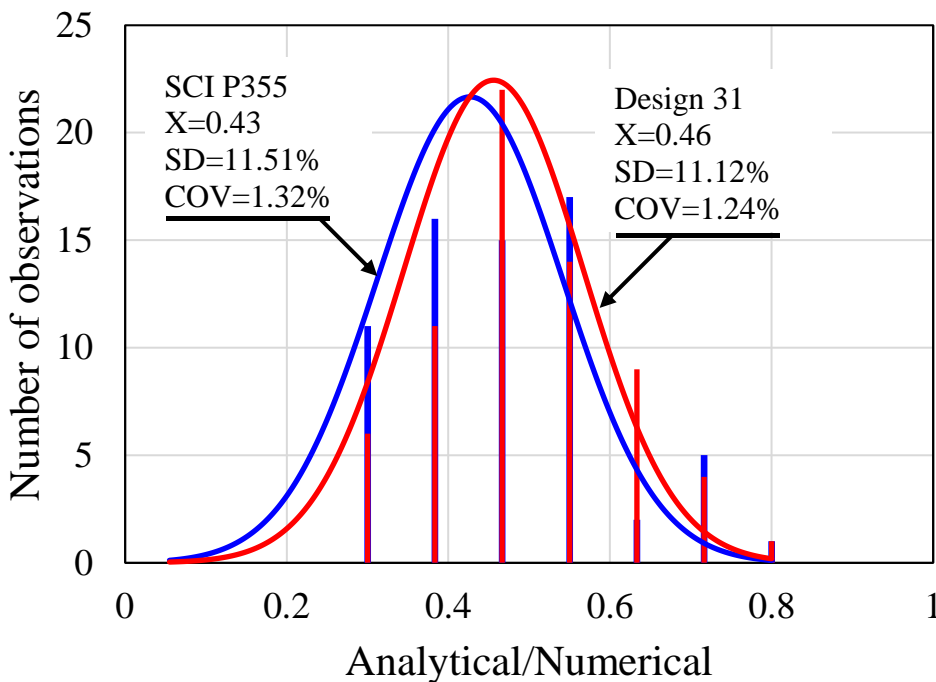


Fig. 34: Scheme for the extraction of the horizontal shear force

579 Next in **Fig. 35**, the results between the numerical and the calculation models are presented. As expected, both calculation
 580 models underestimate the resistance to WPB in composite cellular beams with PCHCS and PCHCSCT. It is worth mentioning that
 581 this has been verified previously in Ferreira et al [7], considering composite slabs, and since the strength of composite cellular beams
 582 with PCHCS and PCHCSCT presented greater resistance than the resistance of composite cellular beams with composite slabs, as
 583 shown in **Fig. 30** and **Fig. 30**, the ratio between the analytical and numerical models tends to be smaller. **Fig. 33** shows the normal
 584 distribution of comparisons between analytical and numerical responses.



585
586 **Fig. 35: Analytical vs. numerical response**



587
588 **Fig. 36: Statistical analyses**

CONCLUSIONS

The present work developed a numerical model capable of predicting the resistance of composite cellular beams with precast hollow core slabs with and without a concrete topping. A parametric study was carried out, considering symmetric, asymmetric sections, as well as key parameters, such as the web-post width and the opening diameter. The models developed were compared with models of composite cellular beams with composite slabs. The failure modes observed were web post buckling (WPB), web post buckling combined with plastic mechanism (WPB+PM), plastic mechanism (PM) and Vierendeel mechanism (VM). In some situations, the shear connector rupture was also observed. This showed that the web post width contributed to the change in the degree of interaction of composite cellular beams. The results showed that the resistance of composite cellular beams is not limited only by the steel cellular profile. In most of the observations, the resistance of composite cellular beams with precast hollow core slabs showed shear resistance equal or greater than the models of composite cellular beams, considering composite slabs. This means that existing calculation models, such as SCI-P355 and Steel Design Guide 31, can be used to design such structural systems. However, the models of composite cellular beams with precast hollow core slabs and concrete topping showed a significant and superior difference when compared with the models of cellular beams associated with composite slabs. Therefore, in this situation, the use of current calculation models can underestimate the strength of composite cellular beams with precast hollow core slabs and concrete topping. This is due to the fact that the hollow core slab with concrete topping presented greater resistance to shear stress.

ACKNOWLEDGMENTS

The authors would like to thank Construção Metálica – Gerdau Aços Brasil for making available the data related to COPPETEC, PEC-18541. This work was supported by the São Paulo Research Foundation (FAPESP) [grant number #2018/22803-1].

REFERENCES

- [1] I.M. Ahmed, K.D. Tsavdaridis, The evolution of composite flooring systems: applications, testing, modelling and eurocode design approaches, *J. Constr. Steel Res.* 155 (2019) 286–300. <https://doi.org/10.1016/j.jcsr.2019.01.007>.
- [2] S. De Nardin, A. El Debs, State of the art of steel–concrete composite structures in Brazil, *Proc. Inst. Civ. Eng. - Civ. Eng.* 166 (2013) 20–27. <https://doi.org/10.1680/cien.2013.166.6.20>.
- [3] D. Lam, Capacities of headed stud shear connectors in composite steel beams with precast hollowcore slabs, *J. Constr. Steel Res.* 63 (2007) 1160–1174. <https://doi.org/10.1016/j.jcsr.2006.11.012>.
- [4] F.D. Queiroz, P.C.G.S. Vellasco, D.A. Nethercot, Finite element modelling of composite beams with full and partial shear connection, *J. Constr. Steel Res.* 63 (2007) 505–521. <https://doi.org/10.1016/j.jcsr.2006.06.003>.
- [5] I.S. Ibrahim, K.S. Elliott, R. Abdullah, A.B.H. Kueh, N.N. Sarbini, Experimental study on the shear behaviour of precast

- 623 concrete hollow core slabs with concrete topping, *Eng. Struct.* 125 (2016) 80–90.
624 <https://doi.org/10.1016/j.engstruct.2016.06.005>.
- 625 [6] E. Baran, Effects of cast-in-place concrete topping on flexural response of precast concrete hollow-core slabs, *Eng. Struct.*
626 98 (2015) 109–117. <https://doi.org/10.1016/j.engstruct.2015.04.017>.
- 627 [7] F.P.V. Ferreira, C.H. Martins, S. De Nardin, Assessment of web post buckling resistance in steel-concrete composite cellular
628 beams, *Thin-Walled Struct.* 158 (2021) 106969. <https://doi.org/10.1016/j.tws.2020.106969>.
- 629 [8] P. Panedpojaman, T. Thepchatri, S. Limkatanyu, Novel design equations for shear strength of local web-post buckling in
630 cellular beams, *Thin-Walled Struct.* 76 (2014) 92–104. <https://doi.org/10.1016/j.tws.2013.11.007>.
- 631 [9] K.D. Tsavdaridis, C. D’Mello, Web buckling study of the behaviour and strength of perforated steel beams with different
632 novel web opening shapes, *J. Constr. Steel Res.* 67 (2011) 1605–1620. <https://doi.org/10.1016/j.jcsr.2011.04.004>.
- 633 [10] F. Erdal, M.P. Saka, Ultimate load carrying capacity of optimally designed steel cellular beams, *J. Constr. Steel Res.* 80
634 (2013) 355–368. <https://doi.org/10.1016/j.jcsr.2012.10.007>.
- 635 [11] L.F. Grilo, R.H. Fakury, A.L.R. de Castro e Silva, G. de S. Veríssimo, Design procedure for the web-post buckling of steel
636 cellular beams, *J. Constr. Steel Res.* 148 (2018) 525–541. <https://doi.org/10.1016/j.jcsr.2018.06.020>.
- 637 [12] D. Kerdal, D.A. Nethercot, Failure modes for castellated beams, *J. Constr. Steel Res.* 4 (1984) 295–315.
638 [https://doi.org/10.1016/0143-974X\(84\)90004-X](https://doi.org/10.1016/0143-974X(84)90004-X).
- 639 [13] K.F. Chung, T.C.H. Liu, A.C.H. Ko, Investigation on vierendeel mechanism in steel beams with circular web openings, *J.*
640 *Constr. Steel Res.* 57 (2001) 467–490. [https://doi.org/10.1016/S0143-974X\(00\)00035-3](https://doi.org/10.1016/S0143-974X(00)00035-3).
- 641 [14] P. Panedpojaman, T. Rongram, Design Equations for Vierendeel Bending of Steel Beams with Circular Web Openings,
642 *World Congr. Eng. 2014. II* (2014) 0–5.
- 643 [15] R. Redwood, S.H. Cho, Design of steel and composite beams with web openings, *J. Constr. Steel Res.* 25 (1993) 23–41.
644 [https://doi.org/10.1016/0143-974X\(93\)90050-3](https://doi.org/10.1016/0143-974X(93)90050-3).
- 645 [16] K.D. Tsavdaridis, C. D’Mello, Vierendeel Bending Study of Perforated Steel Beams with Various Novel Web Opening
646 Shapes through Nonlinear Finite-Element Analyses, *J. Struct. Eng.* 138 (2012) 1214–1230.
647 [https://doi.org/10.1061/\(asce\)st.1943-541x.0000562](https://doi.org/10.1061/(asce)st.1943-541x.0000562).
- 648 [17] R.M. Lawson, J.B.P. Lim, S.O. Popo-Ola, Pull-out forces in shear connectors in composite beams with large web openings,
649 *J. Constr. Steel Res.* 87 (2013) 48–59. <https://doi.org/10.1016/j.jcsr.2013.03.025>.
- 650 [18] R.M.M. Lawson, J. Lim, S.J.J. Hicks, W.I.I. Simms, Design of composite asymmetric cellular beams and beams with large
651 web openings, *J. Constr. Steel Res.* 62 (2006) 614–629. <https://doi.org/10.1016/j.jcsr.2005.09.012>.
- 652 [19] R.M. Lawson, S.J. Hicks, Design of composite beams with large web openings, The Steel Construction Institute, 2011.
- 653 [20] S.S. Fares, J. Coulson, D.W. Dinehart, AISC Steel Design Guide 31: Castellated and Cellular Beam Design, American
654 Institute of Steel Construction, 2016.
- 655 [21] F.P.V.F.P.V.F.P.V. Ferreira, C.H.C.H. Martins, S. De Nardin, Advances in composite beams with web openings and
656 composite cellular beams, *J. Constr. Steel Res.* 172 (2020) 106182. <https://doi.org/10.1016/j.jcsr.2020.106182>.
- 657 [22] D. Lam, Composite steel beams using precast concrete hollow core floor slabs, 1998. Ph.D. thesis. University of
658 Nottingham, 1998.
- 659 [23] E. Ellobody, D. Lam, Modelling of headed stud in steel-precast composite beams, *Steel Compos. Struct.* 2 (2002) 355–378.
660 <https://doi.org/10.12989/scs.2002.2.5.355>.
- 661 [24] D. Lam, K.S. Elliott, D.A. Nethercot, Experiments on composite steel beams with precast concrete hollow core floor slabs,
662 *Proc. Inst. Civ. Eng. - Struct. Build.* 140 (2000) 127–138. <https://doi.org/10.1680/stbu.2000.140.2.127>.
- 663 [25] D. Lam, K.S. Elliott, D.A. Nethercot, Parametric study on composite steel beams with precast concrete hollow core floor
664 slabs, *J. Constr. Steel Res.* 54 (2000) 283–304. [https://doi.org/10.1016/S0143-974X\(99\)00049-8](https://doi.org/10.1016/S0143-974X(99)00049-8).
- 665 [26] D. Lam, Designing composite beams with precast hollowcore slabs to Eurocode 4, *Adv. Steel Constr.* 3 (2007) 594–606.
666 <https://doi.org/10.18057/IJASC.2007.3.2>.

- 667 [27] S.J. Hicks, R.M. Lawson, Design of composite beams using precast concrete slabs., The Steel Construction Institute, 2003.
- 668 [28] G.H. Gouchman, Design of composite beams using precast concrete slabs in accordance with EUROCODE 4, The Steel
669 Construction Institute, 2014.
- 670 [29] EUROPEAN COMMITTEE FOR STANDARDIZATION, EN 1994-1-1: Eurocode 4 – Design of composite steel and
671 concrete structures – Part 1-1: General rules for buildings., (2004).
- 672 [30] E.M. Batista, A. Landesmann, Análise experimental de vigas mistas de aço e concreto compostas por lajes alveolares e
673 perfis laminados. COPPETEC, PEC-18541, (2016).
- 674 [31] F.P.V.F.P.V. Ferreira, C.H.C.H. Martins, S. De Nardin, A parametric study of steel-concrete composite beams with hollow
675 core slabs and concrete topping, Structures. 28 (2020) 276–296. <https://doi.org/10.1016/j.istruc.2020.08.045>.
- 676 [32] C.J. Granade, An investigation of composite beams having large rectangular openings in their webs, 1968. Partial M.Sc.
677 thesis. University of Alabama, 1968.
- 678 [33] W.C. Clawson, D. Darwin, Composite beams with web openings, ASCE J. Struct. Div. 108 (1982) 145–162.
- 679 [34] W.C. Clawson, D. Darwin, Strength of composite beams at web openings, ASCE J. Struct. Div. 108 (1982) 623–641.
- 680 [35] S.H. Cho, An investigation on the strength of composite beams with web openings, 1982. M.Sc. thesis. Hanyang University,
681 1982.
- 682 [36] R. Narayanan, R.I.M. Al-Amery, T.M. Roberts, Shear strength of composite plate girders with rectangular web cut-outs, J.
683 Constr. Steel Res. 12 (1989) 151–166. [https://doi.org/10.1016/0143-974X\(89\)90030-8](https://doi.org/10.1016/0143-974X(89)90030-8).
- 684 [37] T.M. Roberts, R.I.M. Al-Amery, Shear strength of composite plate girders with web cutouts, J. Struct. Eng. 117 (1991)
685 1897–1910. [https://doi.org/10.1061/\(ASCE\)0733-9445\(1991\)117:7\(1897\)](https://doi.org/10.1061/(ASCE)0733-9445(1991)117:7(1897)).
- 686 [38] D.M. Todd, P.B. Cooper, Strength of composite beams with web openings, ASCE J. Struct. Div. 106 (1980) 431–444.
- 687 [39] C.M. DONOGHUE, Strength of composite beams with web openings, ASCE J. Struct. Div. 108 (1982) 2652–2667.
- 688 [40] R.G. Redwood, P.K. Wong, Web holes in composite beams with steel deck, in: Can. Struct. Eng. Conf. -1982, Canadian
689 Steel Construction Council, Ontario, Toronto, 1982: pp. 1–41.
- 690 [41] E.H. Fahmy, Analysis of composite beams with rectangular web openings, J. Constr. Steel Res. 37 (1996) 47–62.
691 [https://doi.org/10.1016/0143-974X\(95\)00022-N](https://doi.org/10.1016/0143-974X(95)00022-N).
- 692 [42] M.A. Benitez, D. Darwin, R.C. Donahey, Deflections of composite beams with web openings, J. Struct. Eng. 124 (1998)
693 1139–1147. [https://doi.org/10.1061/\(ASCE\)0733-9445\(1998\)124:10\(1139\)](https://doi.org/10.1061/(ASCE)0733-9445(1998)124:10(1139)).
- 694 [43] K.. Chung, R.. Lawson, Simplified design of composite beams with large web openings to Eurocode 4, J. Constr. Steel Res.
695 57 (2001) 135–164. [https://doi.org/10.1016/S0143-974X\(00\)00011-0](https://doi.org/10.1016/S0143-974X(00)00011-0).
- 696 [44] R.G. Redwood, G. Poubouras, Tests of composite beams with web holes, Can. J. Civ. Eng. 10 (1983) 713–721.
697 <https://doi.org/10.1139/l83-100>.
- 698 [45] R.C. Donahey, D. Darwin, Web openings in composite beams with ribbed slabs, J. Struct. Eng. 114 (1988) 518–534.
699 [https://doi.org/10.1061/\(ASCE\)0733-9445\(1988\)114:3\(518\)](https://doi.org/10.1061/(ASCE)0733-9445(1988)114:3(518)).
- 700 [46] R.M. Lawson, K.F. Chung, A.M. Price, Tests on composite beams with large web openings to justify existing design
701 methods, Struct. Engineer. 70 (1992) 1–7.
- 702 [47] S.H. Cho, R.G. Redwood, Slab behavior in composite beams at openings. II: tests and verification, J. Struct. Eng. 118 (1992)
703 2304–2322. [https://doi.org/10.1061/\(ASCE\)0733-9445\(1992\)118:9\(2304\)](https://doi.org/10.1061/(ASCE)0733-9445(1992)118:9(2304)).
- 704 [48] J.W. Park, C.H. Kim, S.C. Yang, Ultimate Strength of Ribbed Slab Composite Beams with Web Openings, J. Struct. Eng.
705 129 (2003) 810–817. [https://doi.org/10.1061/\(asce\)0733-9445\(2003\)129:6\(810\)](https://doi.org/10.1061/(asce)0733-9445(2003)129:6(810)).
- 706 [49] R.G. Redwood, G. Poubouras, Analysis of composite beams with web openings, J. Struct. Eng. 110 (1984) 1949–1958.
707 [https://doi.org/10.1061/\(ASCE\)0733-9445\(1984\)110:9\(1949\)](https://doi.org/10.1061/(ASCE)0733-9445(1984)110:9(1949)).
- 708 [50] D. Darwin, R.C. Donahey, LRFD for composite beams with unreinforced web openings, J. Struct. Eng. 114 (1988) 535–
709 552. [https://doi.org/10.1061/\(ASCE\)0733-9445\(1988\)114:3\(535\)](https://doi.org/10.1061/(ASCE)0733-9445(1988)114:3(535)).

- 710 [51] S.H. Cho, R.G. Redwood, Slab behavior in composite beams at openings. I: analysis, *J. Struct. Eng.* 118 (1992) 2287–2303.
711 [https://doi.org/10.1061/\(ASCE\)0733-9445\(1992\)118:9\(2287\)](https://doi.org/10.1061/(ASCE)0733-9445(1992)118:9(2287)).
- 712 [52] K.D. Tsavdaridis, C. D’Mello, M. Hawes, Experimental study of ultra shallow floor beams (USFB) with perforated steel
713 sections, in: *11th Nord. Steel Constr. Conf. 2009 (NSCC 2009)*, Malmö, Sweden, 2009: pp. 312–319.
- 714 [53] C. Maraveas, Z. Fasoulakis, K.D. Tsavdaridis, Fire Resistance of Axially Restrained and Partially Unprotected Ultra
715 Shallow Floor Beams (USFB) and DELTABEAM Composite Beams, in: *Appl. Fire Eng. - Proc. Int. Conf. Appl. Struct.
716 Fire Eng. Conf.*, Manchester, U.K, 2017: pp. 7–8.
- 717 [54] R. Kansinalli, K. Tsavdaridis, Vibration Response of USFB Composite Floors, in: *13th Nord. Steel Constr. Conf. (NSCC
718 2015)*, Tampere, Finland, 2015: pp. 187–188.
- 719 [55] K.D. Tsavdaridis, C. D’Mello, B.Y. Huo, Experimental and computational study of the vertical shear behaviour of partially
720 encased perforated steel beams, *Eng. Struct.* 56 (2013) 805–822. <https://doi.org/10.1016/j.engstruct.2013.04.025>.
- 721 [56] C. Maraveas, K.D. Tsavdaridis, A. Nadjai, Fire Resistance of Unprotected Ultra Shallow Floor Beams (USFB): A Numerical
722 Investigation, *Fire Technol.* 53 (2017) 609–627. <https://doi.org/10.1007/s10694-016-0583-5>.
- 723 [57] O. Hechler, C. Müller, G. Sedlacek, Investigations on Beams with Multiple Regular Web Openings, in: *Compos. Constr.
724 Steel Concr. V*, American Society of Civil Engineers, Reston, VA, 2006: pp. 270–281.
725 [https://doi.org/10.1061/40826\(186\)26](https://doi.org/10.1061/40826(186)26).
- 726 [58] C. MÜLLER, O. HECHLER, A. BUREAU, D. BITAR, D. JOYEUX, L.G. CAJOT, T. DEMARCO, R.M. LAWSON, S.
727 HICKS, P. DEVINE, O. LAGERQVIST, E. HEDMAN-PÉTURSSON, E. UNOSSON, M. FELDMANN, Large web
728 openings for service integration in composite floors. Technical Steel Research. European Comission, Contract No 7210-
729 PR/315. Final report, (2006).
- 730 [59] A. Nadjai, Performance of cellular composite floor beams at ambient temperature, 2005.
- 731 [60] T. Sheehan, X. Dai, D. Lam, E. Aggelopoulos, M. Lawson, R. Obiala, Experimental study on long spanning composite
732 cellular beam under flexure and shear, *J. Constr. Steel Res.* 116 (2016) 40–54. <https://doi.org/10.1016/j.jcsr.2015.08.047>.
- 733 [61] A. Nadjai, O. Vassart, F. Ali, D. Talamona, A. Allam, M. Hawes, Performance of cellular composite floor beams at elevated
734 temperatures, *Fire Saf. J.* 42 (2007) 489–497. <https://doi.org/10.1016/j.firesaf.2007.05.001>.
- 735 [62] Dassault Systèmes Simulia, Abaqus 6.18, (2016).
- 736 [63] M. Sjaarda, T. Porter, J.S. West, S. Walbridge, Fatigue Behavior of Welded Shear Studs in Precast Composite Beams, *J.
737 Bridg. Eng.* 22 (2017) 04017089. [https://doi.org/10.1061/\(ASCE\)BE.1943-5592.0001134](https://doi.org/10.1061/(ASCE)BE.1943-5592.0001134).
- 738 [64] E. El-Lobody, D. Lam, Finite Element Analysis of Steel-Concrete Composite Girders, *Adv. Struct. Eng.* 6 (2003) 267–281.
739 <https://doi.org/10.1260/136943303322771655>.
- 740 [65] F.P.V.F.P.V.F.P.V. Ferreira, A. Rossi, C.H.C.H.C.H. Martins, Lateral-torsional buckling of cellular beams according to the
741 possible updating of EC3, *J. Constr. Steel Res.* 153 (2019) 222–242. <https://doi.org/10.1016/j.jcsr.2018.10.011>.
- 742 [66] F.P.V.F.P.V. Ferreira, C.H.C.H. Martins, LRFD for Lateral-Torsional Buckling Resistance of Cellular Beams, *Int. J. Civ.
743 Eng.* 18 (2020) 303–323. <https://doi.org/10.1007/s40999-019-00474-7>.
- 744 [67] A. Rossi, F.P.V.F.P.V. Ferreira, C.H.C.H. Martins, E.C.E.C. Mesacasa Júnior, Assessment of lateral distortional buckling
745 resistance in welded I-beams, *J. Constr. Steel Res.* 166 (2020) 105924. <https://doi.org/10.1016/j.jcsr.2019.105924>.
- 746 [68] F.P.V.F.P.V. Ferreira, C.H.C.H. Martins, S. De Nardin, Sensitivity Analysis of Composite Cellular Beams to Constitutive
747 Material Models and Concrete Fracture, *Int. J. Struct. Stab. Dyn.* (2020) 2150008.
748 <https://doi.org/10.1142/S0219455421500085>.
- 749 [69] S. Chen, Y. Jia, Numerical investigation of inelastic buckling of steel–concrete composite beams prestressed with external
750 tendons, *Thin-Walled Struct.* 48 (2010) 233–242. <https://doi.org/10.1016/j.tws.2009.10.009>.
- 751 [70] W.-B. Zhou, W.-J. Yan, Refined nonlinear finite element modelling towards ultimate bending moment calculation for
752 concrete composite beams under negative moment, *Thin-Walled Struct.* 116 (2017) 201–211.
753 <https://doi.org/10.1016/j.tws.2017.02.011>.
- 754 [71] A. Hillerborg, M. Modéer, P.-E. Petersson, Analysis of crack formation and crack growth in concrete by means of fracture
755 mechanics and finite elements, *Cem. Concr. Res.* 6 (1976) 773–781. [https://doi.org/10.1016/0008-8846\(76\)90007-7](https://doi.org/10.1016/0008-8846(76)90007-7).

- 756 [72] J. Lubliner, J. Oliver, S. Oller, E. Oñate, A plastic-damage model for concrete, *Int. J. Solids Struct.* 25 (1989) 299–326.
757 [https://doi.org/10.1016/0020-7683\(89\)90050-4](https://doi.org/10.1016/0020-7683(89)90050-4).
- 758 [73] J. Lee, G.L. Fenves, Plastic-Damage Model for Cyclic Loading of Concrete Structures, *J. Eng. Mech.* 124 (1998) 892–900.
759 [https://doi.org/10.1061/\(ASCE\)0733-9399\(1998\)124:8\(892\)](https://doi.org/10.1061/(ASCE)0733-9399(1998)124:8(892)).
- 760 [74] T. Yu, J.G. Teng, Y.L. Wong, S.L. Dong, Finite element modeling of confined concrete-I: Drucker–Prager type plasticity
761 model, *Eng. Struct.* 32 (2010) 665–679. <https://doi.org/10.1016/j.engstruct.2009.11.014>.
- 762 [75] D.J. CARREIRA, K.H. CHU, Stress-Strain Relationship for Plain Concrete in Compression, *ACI J. Proc.* 82 (1985) 797–
763 804. <https://doi.org/10.14359/10390>.
- 764 [76] D.J. Carreira, K.H. Chu, Stress-Strain Relationship for Reinforced Concrete in Tension., *J. Am. Concr. Inst.* 83 (1986) 21–
765 28.
- 766 [77] D.L. Araújo, M.W.R. Sales, S.M. Paulo, A.L.H.C. El Debs, Headed steel stud connectors for composite steel beams with
767 precast hollow-core slabs with structural topping, *Eng. Struct.* 107 (2016) 135–150.
768 <https://doi.org/10.1016/j.engstruct.2015.10.050>.
- 769 [78] X. Yun, L. Gardner, Stress-strain curves for hot-rolled steels, *J. Constr. Steel Res.* 133 (2017) 36–46.
770 <https://doi.org/10.1016/j.jcsr.2017.01.024>.
- 771 [79] S. Wijesiri Pathirana, B. Uy, O. Mirza, X. Zhu, Flexural behaviour of composite steel–concrete beams utilising blind bolt
772 shear connectors, *Eng. Struct.* 114 (2016) 181–194. <https://doi.org/10.1016/j.engstruct.2016.01.057>.
- 773 [80] U. Katwal, Z. Tao, M.K. Hassan, B. Uy, D. Lam, Load sharing mechanism between shear studs and profiled steel sheeting
774 in push tests, *J. Constr. Steel Res.* 174 (2020) 106279. <https://doi.org/10.1016/j.jcsr.2020.106279>.
- 775 [81] X. Liu, M.A. Bradford, Q.-J. Chen, H. Ban, Finite element modelling of steel–concrete composite beams with high-strength
776 friction-grip bolt shear connectors, *Finite Elem. Anal. Des.* 108 (2016) 54–65. <https://doi.org/10.1016/j.finel.2015.09.004>.
- 777 [82] S. Guezouli, A. Lachal, Numerical analysis of frictional contact effects in push-out tests, *Eng. Struct.* 40 (2012) 39–50.
778 <https://doi.org/10.1016/j.engstruct.2012.02.025>.
- 779 [83] Y. Chen, Innovative shear connections for the accelerated construction of composite bridges, 2013. Ph.D. thesis. University
780 of Waterloo, 2013.
- 781 [84] T.N.H. Nguyen, K.H. Tan, T. Kanda, Investigations on web-shear behavior of deep precast, prestressed concrete hollow
782 core slabs, *Eng. Struct.* 183 (2019) 579–593. <https://doi.org/10.1016/j.engstruct.2018.12.052>.
- 783 [85] Sameer S. Fares, J. Coulson, David W. Dinehart, Castellated and Cellular Beam Design 31, *Am. Inst. Steel Constr.* (2016).
- 784 [86] American Institute of Steel Construction, ANSI/AISC 360-16 - Specification for structural steel buildings., (2016).
- 785